# Efficient Chromium (VI) Removal from Wastewater by Adsorption-assisted Photocatalysis using MXene

Nur Shafiqah Jamaluddin[a], Nur Hashimah Alias[a]*, Sadaki Samitsu[b], Nur Hidayati Othman[a], Juhana Jaafar[c], Fauziah Marpani[a] and Woei Jye Lau[c]

[a]*Department of Oil and Gas Engineering, School of Chemical Engineering, College of Engineering, Universiti Teknologi MARA, 40450 Shah Alam, Selangor, Malaysia*
[b]*Research and Services Division of Materials Data and Integrated System (MaDIS), National Institute for Materials Science (NIMS), 1-2-1 Sengen, Tsukuba, Ibaraki 305-0047, Japan*
[c]*Advanced Membrane Technology Research Centre (AMTEC), School of Chemical and Energy Engineering, Faculty of Engineering, Universiti Teknologi Malaysia, 81310 Skudai, Johor, Malaysia*

*Corresponding author: nurhashimah@uitm.edu.my

## Abstract

Hexavalent chromium (Cr(VI)) is considered hazardous heavy metal in water bodies that can cause severe effects on human health and the environment. Over the years, myriad attention has been focused on developing photocatalyst materials to remove Cr(VI) from wastewater. However, the broad bandgap energy and high electron recombination rate of these conventional photocatalysts have limited their photocatalytic ability. Therefore, efficient photocatalytic materials for Cr(VI) removal in wastewater is strongly demanded. In this study, delaminated MXene was successfully synthesised and removed Cr(IV) from aqueous solution. The synthesised delaminated MXene was characterised using XRD, EDX, FTIR, FESEM, nitrogen adsorption-desorption analysis, TGA, UV-Vis-NIR spectroscopy and XPS. Based on the results, the optimum operating conditions on Cr(VI) removal by the synthesised MXene was obtained at pH 4 with photocatalyst loading of 1.5 g/L, and Cr(VI) concentration of 5 mg/L. The removal efficiency of Cr(VI) via adsorption-assisted photocatalysis over various concentrations was approximately 3.1%–28.9% higher than adsorption, verifying a synergistic effect of adsorption and photocatalysis by the delaminated MXene. The isotherm of Cr(VI) adsorption was fitted by the Langmuir model ($R^2 > 0.9848$), which is better than the Freundlich model ($R^2 > 0.8824$). Meanwhile, the time

dependence of Cr(VI) adsorption was well fitted to pseudo-second-order kinetic model with $R^2 > 0.9999$, which is 2.8 times higher with respect to MXene. In conclusion, the results obtained suggest that the delaminated MXene possesses excellent ability to remove Cr(VI) via adsorption-assisted photocatalysis and has a great potential to be used for industrial wastewater applications.

**Keywords:** MXene; chromium (VI); adsorption; photocatalysis; wastewater

## 1.0 Introduction

In recent years, significant improvement of water purification technology has been strongly demanded because a large volume of wastewater containing heavy metals is discharged in many industrial processes such as electroplating, metal coating, electropolishing, inferior cosmetic raw materials, and leather tanning [1,2]. Chromium is one of the most prevalent heavy metals in industrial wastewater, which mainly exists as Cr(VI) and Cr(III) [3]. The toxicity of the ions depends on their valency and coordination number. Cr(III) is relatively less harmful as it has low mobility in water and soil. It is also known as an essential micronutrient to maintain the metabolism of proteins, lipids, and sugars in the human body [1,4]. Oppositely, Cr(VI) is highly toxic, leading to serious health issues such as kidney failure, skin sensitivity, lung cancer, genetic defects, liver damage, and even death [4–6]. Therefore, according to the World Health Organization (WHO) recommendation, the maximum tolerable concentration of Cr(VI) in drinking water should not exceed 0.05 mg/L [5]. In this regard, separation and purification technology are necessary for the chemical engineering field to eliminate Cr(VI) and convert it to less toxic trivalent chromium, Cr(III), from effluent wastewater. Various approaches have been examined to remove Cr(VI) including ion exchange [7,8], chemical precipitation [9], membrane process [10,11], electrochemical treatment [12], adsorption [11,13], and photocatalysis [14–17]. Photocatalysis assisted by nanomaterials is a promising method for the purification process of ion-contaminated wastewater. The nanomaterials effectively capture water-soluble harmful ions via physical and chemical adsorption and can transform the ions into another less harmful ion species by photo-assisted chemical reaction. The process is favourable as separation and purification methods owing to high removal efficiency, environmental friendliness, and low energy cost [15]. A recent study demonstrated that Zn-Al-layered double hydroxide and $TiO_2$ composites have higher

efficiency for Cr(VI) removal than simple adsorption [18]. According to this study, several photocatalytic adsorbents have been examined for Cr(VI) removal from wastewater: metal sulphide [19,20], zinc oxide [17,21], and titanium dioxide [16,22]. However, they possess some limitations and poor photocatalysis performance due to the broad bandgap energy and high electron recombination rate of the photocatalysts. Therefore, an efficient photocatalytic adsorbent effective for Cr(VI) removal in wastewater is strongly demanded [23].

In 2011, a new member of two-dimensional (2D) nanomaterial, called MXene, was discovered by Naquib et al. from Drexel University [24], comprising transition metal carbides, carbonitrides, and nitrides [25]. MXene is denoted by a general formula of $Mn+1X_nT_x$ where M represents the transition metals, X represents either carbon or nitrogen, n represents any number (n = 1, 2, 3,…), and $T_x$ is surface functional groups (–O, –OH, –Cl, or –F) [26–29]. The MXene has attracted extensive attention owing to its porous structure, water affinity, superior electrical conductivity, excellent structural stabilities, tunable interlayer spacing [30,31], sufficient bandgaps energy [32–35]. In addition, MXene was provenly efficient for the adsorption of dyes and heavy metal ions such as Cu(II) [36], Pb(II) [37], Hg(II) [38,39], and Cr(VI) [40–42]. Mashtalir et al.[43] reported that MXene can be used as a photocatalyst to enhance the photodegradation of MB and AB80 dyes. Furthermore, MXene behaves as a photocatalyst for arsenic (As) species and 94% removal of As species was demonstrated under ultraviolet (UV)-light irradiation [44]. Recently, a few-layer MXene sheets structure, commonly called delaminated MXene, was synthesized by intercalating $Ti_3C_2T_x$ surface with suitable solvent followed by bath sonication [45]. The reported adsorption capacity of delaminated MXene for Pb(II) removal was 2.7 times higher than commercial activated carbon [45].

Therefore, this study demonstrates the adsorption-assisted photocatalytic ability of delaminated MXene that is effective on Cr(VI) removal in wastewater for the first time. delaminated MXene was prepared by etching the aluminium (Al) constituent from ternary layered carbide ($Ti_3AlC_2$) and was characterized by its physicochemical and thermal properties. Cr(VI) removal performance was evaluated by varying pHs, photocatalyst loadings, and Cr(VI) solutions concentration. A possible Cr(VI) removal mechanism via adsorption-assisted photocatalysis was also proposed based on the adsorption isotherm, kinetic study and characterization results of the synthesized delaminated MXene.

## 2.0 Materials and Methods

### *2.1 Materials*

Layered ternary carbide ($Ti_3AlC_2$, MAX) powders (>99 wt % purity) was supplied by Nanoshel (Intelligent Materials Pvt Ltd). Hydrofluoric acid (HF, 49%) and dimethyl sulfoxide (DMSO, 99%) were purchased from Sigma Aldrich Co., Inc. All chemicals were used without further purification. Deionized water was used for washing and experimental works.

### *2.2 Preparation of delaminated MXene ($Ti_3C_2T_x$)*

The preparation of delaminated MXene consists of the etching and delamination process by a method previously reported by [25,44], as schematically illustrated in Scheme 1. In the etching process, 1.0 g graphitic-greyish $Ti_3AlC_2$ consisting of layered MAX phase was gradually immersed in 28 mL of 10 wt % aqueous hydrofluoric acid (HF) in a 60 mL polypropylene (PP) bottle for 24 h under vigorous magnetic stirring. Sedimented solids were collected via centrifugation process at 5000 rpm for 5 min and washed with deionized water to completely remove contaminants until the pH of the dispersion was stabilized around pH 6. The solids were dried in an oven at 70 °C for 24 h, and a few layers of MXene ($Ti_3C_2T_x$) were collected as black solids. In the subsequent delamination process, the MXene was immersed in 12 mL of dimethyl sulfoxide (DMSO) for 20 h at room temperature, followed by bath sonication for 30 min. The delaminated $Ti_3C_2T_x$ was further washed with deionized water and collected by centrifugation at 10000 rpm for 1 hour. The solids were dried at 120 °C for 24 h and collected as black powder, named delaminated MXene hereafter. Overall, approximately 80% yield of delaminated MXene was obtained from $Ti_3AlC_2$.

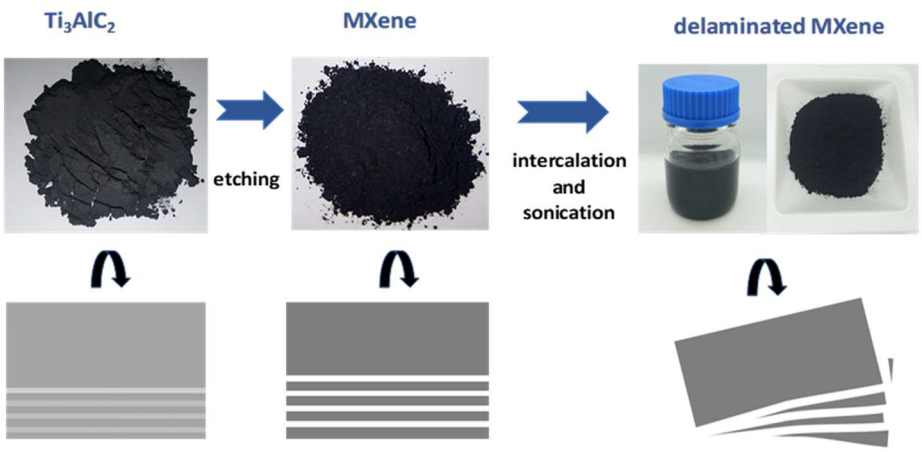

Scheme 1. Schematic illustration of the delaminated MXene synthesis procedure

*2.3 Characterization*

The crystalline structure of $Ti_3AlC_2$ and delaminated MXene were analyzed using X-ray diffraction (XRD, D/Max 2550 PC, Rigaku, Japan) using Cu Kα radiation (wavelength = 0.154 nm) with an accelerating voltage of 40 kV and current of 30 mA. The diffraction patterns were recorded over the diffraction angle 2θ between 2° and 80° at a scan rate of 5°/min. The morphology of $Ti_3AlC_2$ and delaminated MXene was observed using a Field emission scanning electron microscope (FESEM, S-4800, Hitachi High Tech. Co.). The elemental mappings of $Ti_3AlC_2$ and delaminated MXene were quantified using an energy dispersive X-ray analyzer (EDX, Oxford Instruments USA), attached to FESEM. Nitrogen adsorption/desorption measurement was performed using the Micromeritics ASAP 2020 system at −196°C. Prior to the measurement, samples were dried under vacuum at 120 °C for 5 h. The specific surface area of the prepared samples was measured using Brunauer–Emmett–Teller (BET) analysis. The thermal stability of the prepared delaminated MXene was evaluated using a thermogravimetric analyzer (TGA4000, Perkin Elmer Inc.) under nitrogen gas at a heating rate of 10 °C/min to 800 °C. Fourier transform infrared spectroscopy (FTIR, Perkin-Elmer, USA) with transmission configuration was employed to analyze the chemical structure of delaminated MXene before and after Cr(VI) adsorption. The prepared samples were ground with potassium bromide (KBr) at a weight ratio of 1:10 and pressed into pellets to reduce undesirable scattering by air void. Under ambient conditions, FTIR spectra were recorded at the wavenumber range of 500 to 4000 cm−1. The optical band gap of the synthesized delaminated MXene was analyzed by a LAMDATM 1050 UV-Vis-NIR spectrometer along with 150-mm integrating sphere. The band gap energy of the delaminated MXene was estimated using the Kubelka–Munch function by plotting $(\alpha hv)^2$ versus $hv$ [46], where α is the absorption coefficient, and hv is the photon energy. X-ray photoelectron spectroscopy (XPS) measurements were carried out using XPS Quantera II (ULVAC PHI) with X-ray source of Al K$\alpha$ (1486 eV).

*2.4 Adsorption and photocatalysis measurements*

A 1000 mg/L stock solution of Cr(VI) was prepared by dissolving K2Cr2O7 in deionized water and further diluted to a targeted concentration before using it for the adsorption and adsorption-assisted photocatalysis experiments. The Cr(VI) solution was adjusted at the fixed pH between 2–6 using 0.1 M HCl and 0.1 M NaOH. Adsorption of

Cr(VI) without UV-light irradiation was evaluated under dark conditions. Meanwhile, adsorption-assisted photocatalytic experiments were conducted under UV- light irradiation. Before UV-light irradiation on, Cr(VI) solution suspended with photocatalyst was stabilized in the dark for 30 minutes. The schematic illustration of the experiment is depicted in Scheme 2. After a certain period, Cr(VI) concentration was measured using Cary 60 ultraviolet-visible (UV-Vis) spectrophotometer via 1,5-dipenylcarbazide method at a wavelength of 543nm [47]. To quantify the reduction of Cr(VI) at the optimized reaction condition, Atomic absorption spectroscopy (AAS, Z-2000, Hitachi) was also employed to determine the total Cr(III) in the solution. The sample solution was filtered using a polyethersulfone (PES) syringe filter (0.22 μm) before AAS and UV-Vis evaluation. The adsorption capacity and removal percentage were calculated using Eq.1 and Eq.2.

$$\text{Adsorption capacity, (mg/g)} = \frac{c_i - c_e}{\text{m}} V \qquad \text{(Eq. 1)}$$

$$\text{Removal percentage (\%)} = \left(\frac{c_i - c_e}{c_i}\right) \times 100 \qquad \text{(Eq. 2)}$$

Where $c_i$ is the initial Cr(VI) concentration (mg/L), $c_e$ is the final Cr(VI) concentration (mg/L) at their respective times (min), m is the mass of the delaminated MXene (g), and V is the volume of the solution (L).

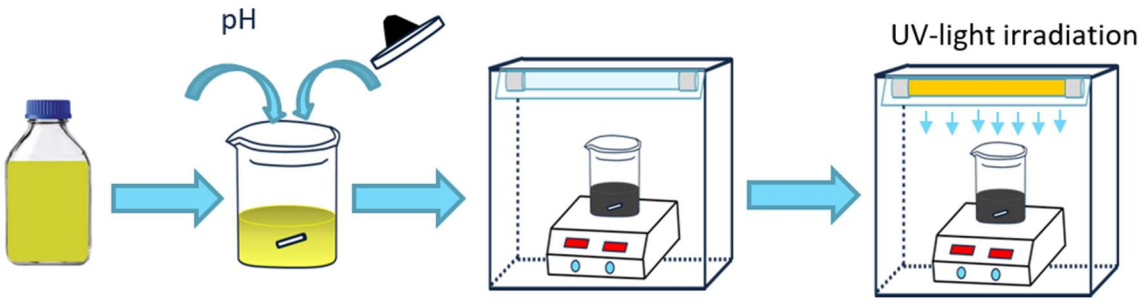


Scheme 2. Schematic illustration of Cr(VI) removal under adsorption-assisted photocatalysis.

Meanwhile, the adsorption isotherm of Cr(VI) was fitted using Langmuir and Freundlich models. The linearized forms of the model equations are expressed by Eq.3 and Eq.4.

Langmuir model

$$\frac{c_e}{q_e} = \frac{1}{K_L q_{max}} + \frac{c_e}{q_{max}} \quad \text{(Eq. 3)}$$

Freundlich model

$$\log q_e = \log K_F + \frac{1}{n} \log c_e \quad \text{(Eq. 4)}$$

Where $c_e$ is the final Cr(VI) concentration (mg/L) at their respective times. $q_e$ (mg/g) is the adsorption capacity of Cr(VI) at equilibrium, $q_{max}$ (mg/g) is the maximum capacity amount of Cr(VI) per unit weight of delaminated MXene, $K_L$ (L/mg) is the Langmuir isotherm constant, and $K_F$(mg/g)(L/mg)(1/n) and n are the Freundlich isotherm constants. The kinetic study of Cr(VI) adsorption was evaluated at the optimal loading of delaminated MXene and Cr(VI) concentration within 7 hour. At every 1-hour interval, a small amount of Cr(VI) solution was extracted and subjected to AAS. The time dependence of the Cr(VI) adsorption experiment was fitted by pseudo-first and pseudo-second-order kinetic models [45–47]. The linear forms of kinetic models are expressed in Eq.5 and Eq.6.

Pseudo-first order kinetic

$$\ln (q_e - q_t) = \ln q_e - k_1 t \quad \text{(Eq. 5)}$$

Pseudo-second-order

$$\frac{t}{q_t} = \frac{1}{k_2 {q_e}^2} + \frac{1}{q_e} \quad \text{(Eq. 5)}$$

where $k_1$ (min-1) and $k_2$ (g/mg.min) are the rate constants and $q_t$ (mg/g), is the adsorption capacity at a specific time t (min).

## 3.0 Results and Discussion

### *3.1 Characterization of MXene*

To evaluate their crystalline structure and interlayer spacing, XRD analysis was carried out for $Ti_3AlC_2$, MXene, and delaminated MXene (Figure 1). $Ti_3AlC_2$ presents an intense peak at 2θ = 39°, corresponding to (104) in $Ti_3AlC_2$. After etching $Ti_3AlC_2$ by 10 wt % HF, MXene, and delaminated MXene lost the (104) peak completely, and a new peak appeared approximately at 27.8° that corresponds to (006) diffraction. An indistinct peak of

TiC impurity was found at 37°. Moreover, the main diffraction peaks of $Ti_3AlC_2$ became weaker and broader after undergoing the etching and delamination processes. The results indicate that etching by 10 wt % HF successfully ruptured the Ti–Al metal bond and removed the Al element in $Ti_3AlC_2$ due to weak bond energy in $Ti_3AlC_2$ [32]. After the delamination process, all the XRD peaks remained, and the observable peak (002) was shifted from 9.4° to 8.9°, confirming an increase in interlayer layer spacing without the loss of significant peaks. Most of the peaks became broad, consistent with the decrease in crystallinity by delamination. A similar observation was reported by other researchers [48].

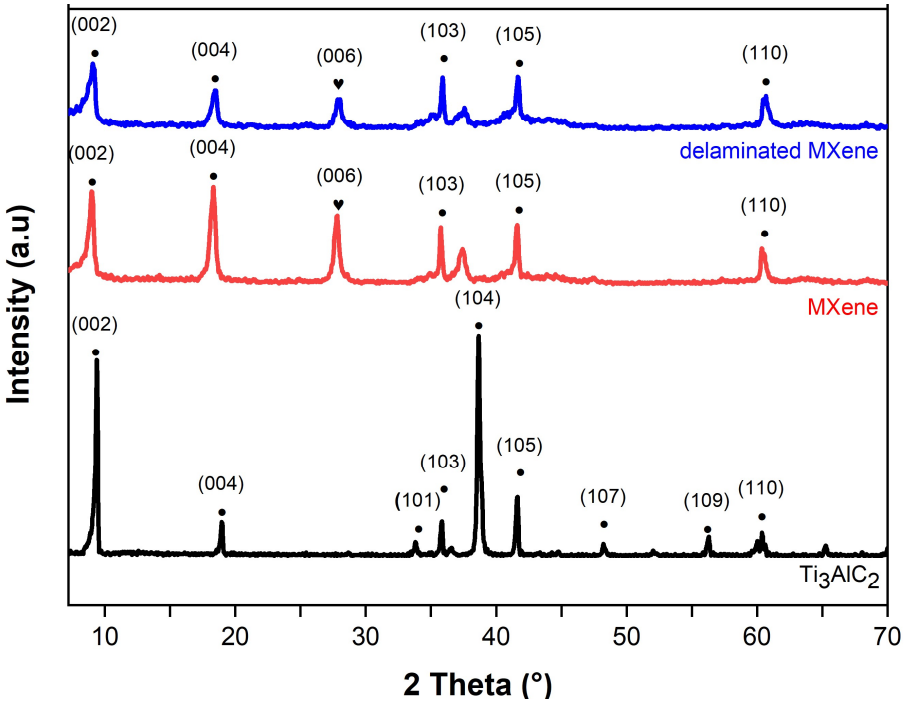


Figure 1. XRD patterns of $Ti_3AlC_2$, MXene, and delaminated MXene.

Based on the EDX spectrum in Figure 2(a and b), the sharp peak of Al in $Ti_3AlC_2$ decreased tremendously after the delamination process. The calculated atomic percentage of Al reduced from 19.5 at% in $Ti_3AlC_2$ to 0.2 at.% in the delaminated MXene. The negligible amount of Al indicates the effective etching process by HF. The synthesized delaminated MXene also displayed the peaks of titanium, Ti (36 at. %), oxygen, O (30.6 at. %), carbon, C (22.9 at. %) and fluorine, F (10.2 at. %). Ti and C are clearly attributed to the elements of $Ti_3AlC_2$, whereas O and F probably are the result of the etching reaction by HF. FTIR analysis was conducted to verify the functional groups of delaminated MXene. As shown in Figure 2c, the peak at 3381 cm−1 is mainly due to the –OH stretching vibrations, whereas the distinctive peak at 1626 cm−1 represents the C=O groups. In addition, the peak at 582

cm−1 is attributed to the Ti–O–Ti bond, and the peak at 1097 cm−1 signifies the deformation vibrations of the C–F bond. These findings were quantitatively confirmed by XPS analysis. Figure 10(a-c) displayed XPS spectra of C 1s, O 1s and Ti 2p in the synthesized delaminated MXene. In C 1s spectrum, the assigning peak at 281.43 represents the Ti-C bond, whereas the other three peaks located at 284.57, 286.01 and 288.53 represents C-C , C-O and O-C = O bonds, respectively. Meanwhile, the O 1s spectrum revealed that the characteristic peaks observed at 530.34, 531.57 and 533.21 eV are assigned to the Ti-O, C=C and C-O bonds, respectively. Ti 2p spectra showed peaks at 455.09 and 459.18, indicating Ti-C and $TiO_2$ or $TiO_2$-x-Fx species.

The observed functional groups detected in the FTIR and XPS spectrum agrees with the elements presented in the EDX result. These results prove that the delaminated MXene contained abundant –OH and small amounts of –F, –OH, and –COOH as terminal groups on the sheet structure in the delaminated MXene. The EDX result showed O was more dominant than F, possibly due to the low concentration of HF used in the etching process. The low concentration of HF was preferable to minimize the terminal groups of –F as the availability of –F can possess hydrophobic characteristics, which might reduce the ability of $Ti_3C_2$ sheets to intercalate with water. Particularly, 10 wt % concentration of HF was strong enough to allow the O/OH ratio as the main terminal group, indicating that Tx was mostly represented by –OH functional groups. These findings agree with previously published research work reported on MXene [49–52]

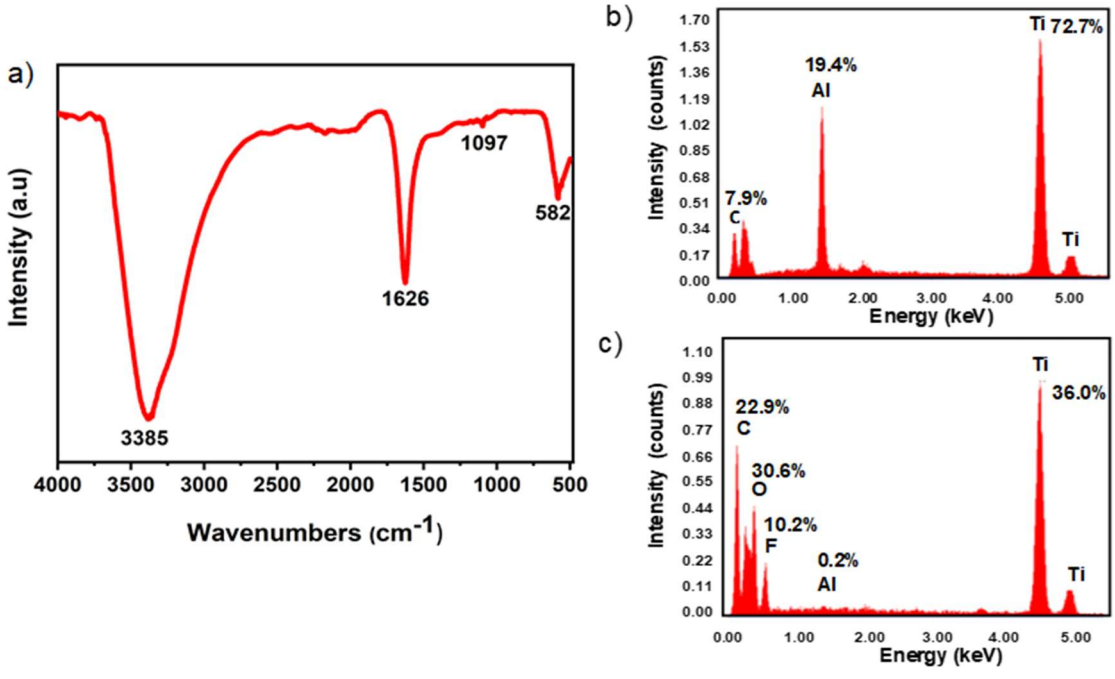

Figure 2. EDX spectrum of a) $Ti_3AlC_2$ b) delaminated MXene (All the peaks were normalized to the peak intensity of Ti and c) FTIR spectrum of delaminated MXene

Figure 3 shows the FESEM images of $Ti_3AlC_2$and delaminated MXene. The top-view surface of $Ti_3AlC_2$ displays an irregular shape structure (Figure 3a), and delaminated MXene has a crumpled shape with numerous ridges and rough surfaces (Figure 3b), which presents the morphological difference of $Ti_3AlC_2$ after the etching and delamination processes. The layered structures of $Ti_3AlC_2$ and delaminated MXene were clearly observed on the magnified SEM images of their cross-section in Figure 3(c and d). Figure 3(d) also reveals the formation of delaminated MXene, yielding a morphology of a few-layer structure with less than 100 nm interlayer spacing which concludes the successful removal of the Al layers from $Ti_3AlC_2$ after the etching and delamination process. Similar findings were also reported elsewhere [39,41].

Nanoporous structures of $Ti_3AlC_2$ and as-synthesized delaminated MXene were evaluated using nitrogen gas adsorption (Figure 3e). MXene and delaminated MXene displayed a type IV isotherm which indicates the delaminated MXene is a mesoporous material, whereas $Ti_3AlC_2$ showed a type I isotherm corresponding to macroporous or non-porous morphology [41]. The specific surface area determined via BET analysis were 1.8 m2/g for $Ti_3AlC_2$ and 4.2 m2/g for MXene. The specific surface area of the synthesized delaminated MXene substantially increased after removing the Al layers using the etching process. Upon delamination, the synthesized delaminated MXene increased to 8.2 m2/g, which in turn increasing the pore volume. These results demonstrated the intercalation of DMSO and bath sonication contributed to enlarging the interlayer space of the synthesized delaminated MXene, facilitating accessible sites for adsorption [41,53]. Therefore, from adsorption and desorption analysis, delaminated MXene adsorbed the highest amount of $N_2$ as compared to MXene and $Ti_3AlC_2$. The increment of the specific surface area is also beneficial to enhance the photocatalytic activity of MXene.

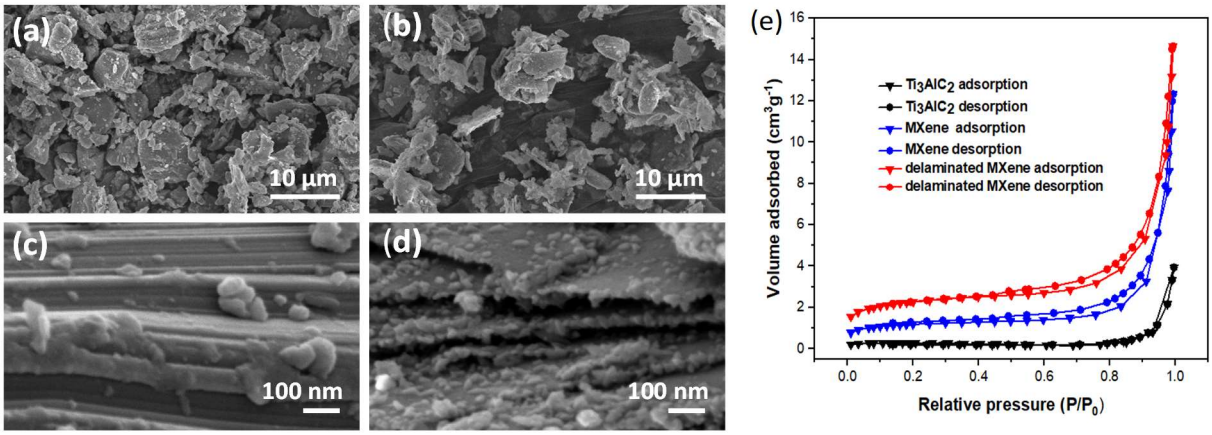


Figure 3 Top-view and cross-sectional FESEM images of (a & c) $Ti_3AlC_2$, (b & d) delaminated MXene and e) Nitrogen adsorption/desorption analysis of $Ti_3AlC_2$ and delaminated MXene.

Besides physicochemical study, thermal and optical analysis was also conducted to evaluate the thermal properties and bandgap of the delaminated MXene. Generally, the thermal degradation of delaminated MXene can be divided into three stages [40,54,55]. The first stage refers to the 4%–5% weight loss of delaminated MXene from room temperature to 200 °C, originating from the adsorbed water molecules on the delaminated MXene surface [54]. The second stage refers to the weight loss at a temperature above 200 °C, which can be ascribed to the degradation of delaminated MXene functional groups like –OH. Moreover, this can also be influenced by the degradation of interlayer ions found on the surface of delaminated MXene. The final mass loss phase was seen between 470 and 700 °C. The calculated percentage of total weight loss was only about 6%–10% and can be delineated to the degradation of layered arrangement of delaminated MXene. These findings demonstrate that delaminated MXene had high thermal properties in terms of thermal stability and thermal degradation. The band gap of delaminated $Ti_3C_2T_x$ MXene successfully investigated by UV-Vis-NIR with integrating sphere accessory as shown in Figure 4. The band gap energy of delaminated MXene was estimated by determining a straight segment of graph. The obtained bandgap energy (Eg) of delaminated MXene was found at 2.26 eV, which is calculated from the which greatly support the photocatalytic activity under visible and UV-light irradiation.

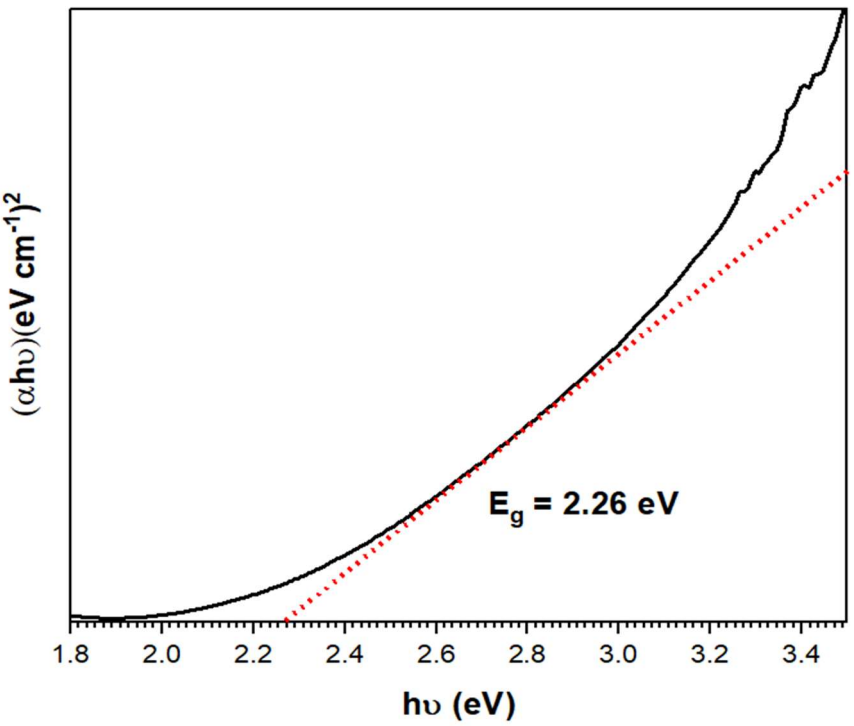


Figure 4 The bandgap energy of delaminated MXene

### *3.2. Synergistic effects of adsorption and photocatalysis*

Cr(VI) removal by delaminated MXene under the adsorption process was compared with the adsorption-assisted photocatalysis process that underwent simultaneous adsorption–photocatalysis processes (Figure 5) over various concentrations. The photocatalysis process showed ascending trend of Cr(VI) removal from 5mg/L to 25 mg/L with 3.1-28.9% increment, respectively. The detailed performance comparison on kinetic removal at 5 mg/L can be seen in Figure 6. Based on the Figure, the adsorption activity demonstrated 81.2% removal at the initial 30 min and reached 96.9% after 7 h reaction under dark conditions, corresponding to the equilibrium point. Under UV-light irradiation, Cr(VI) removal by photocatalysis significantly improved to 97.9% within 30 min, exceeding the Cr(VI) removal without UV light after 7 h. The results reveal that delaminated MXene exhibited faster and higher Cr(VI) removal under UV-light irradiation than without UV-irradiation, indicating the synergistic effect of adsorption and photocatalysis of delaminated MXene.

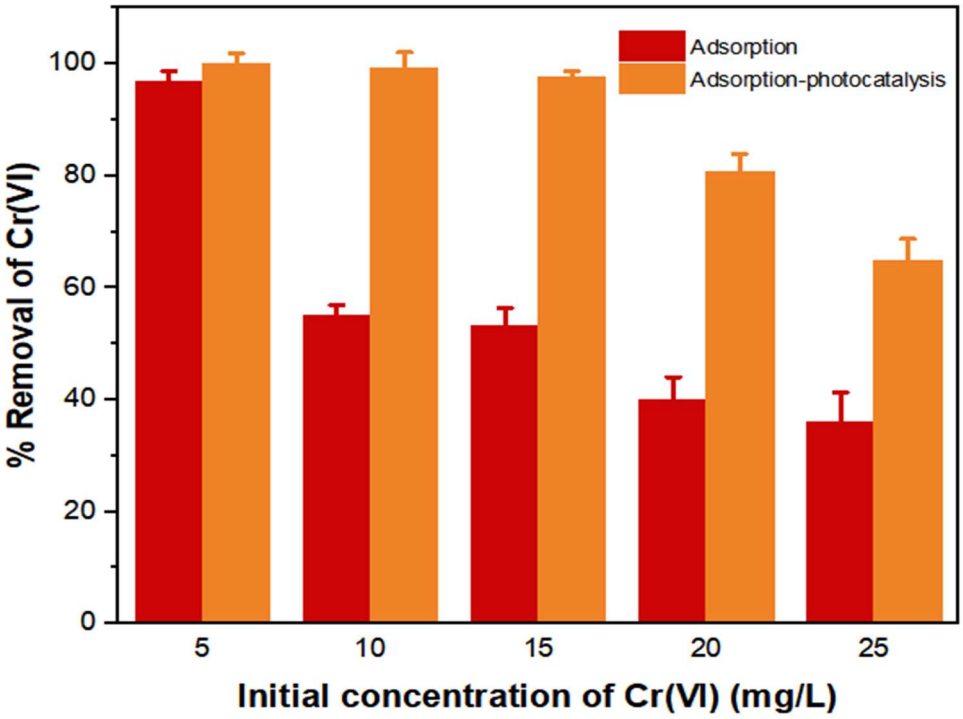


Figure 5. Percentage removal Cr(VI) performance via adsorption and adsorption-assisted photocatalysis over various concentrations.

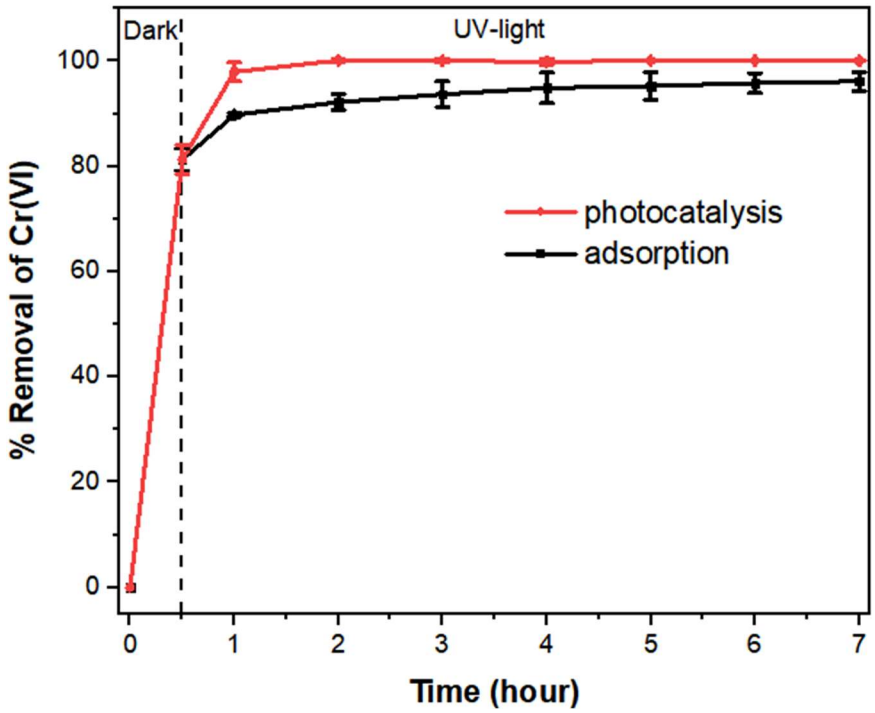


Figure 6. Kinetic of Cr(VI) removal by adsorption and photocatalysis (catalyst dosage 1.5g/L, Cr(VI) concentration 5mg/L pH )

### *3.3. Performance evaluation for operating parameters*

#### *3.3.1. Effect of pH*

The removal of heavy metal ions by adsorption and photocatalysis processes is usually affected by pH since variations in pH have a significant influence on the surface charge, diffusion process, and surface bindings of heavy metals [56]. The point of zero net charge or isoelectric point ($pH_{pzc}$) of delaminated MXene was determined by varying initial pH values (from 2 to 10) using HCl and NaOH. According to the plot of different pH changes, pH initial − pH final ($pH_i$-$pH_f$) versus pH initial ($pH_i$), the $pH_{pzc}$ of delaminated MXene was approximately at pH 5.7 (Figure 7a), which suggests delaminated MXene has a positive surface charge when pH of the solution is less than 5.7. In addition, Cr(VI) have different types of anionic forms depending on pH values. Cr(VI) commonly exists as $Cr_2O_7^{2-}$ and $HCrO_4^-$ under acidic pH range, while under neutral and alkaline conditions, the dominant ionic form of Cr(VI) is $CrO_4^{2-}$ [40].

The effect of initial pH on the removal of Cr(VI) was investigated at three different pH values (pH of 4, 6, and 8). As shown in Figure 7b, the removal efficiency of Cr(VI) decreased significantly from 100% to 67.1%, with increasing initial pH from 4 to 8. This was mainly due to the electrostatic repulsion between Cr(VI) metal ions and the surface charge of the synthesized delaminated MXene at a high pH value [57]. Oppositely, at pH less than 5.7, the negative charge of OH− on the delaminated MXene can be neutralized by positive H+ ions, enhancing the removal of Cr(VI). These results are similar to those reported previously on Cr(VI) removal by rice husk [56].

#### *3.3.2. Effect of photocatalyst loading*

The removal experiment without delaminated MXene exhibited no removal for 7 h, confirming no Cr(VI) self-degradation under UV irradiation. When delaminated MXene was added at the dosage of 1.5 g/L, the removal efficiency of Cr(VI) at equilibrium increased significantly to 100% due to enough exchangeable sites available for Cr(VI) removal. Moreover, the increment of delaminated MXene until 1.5 g/L can be related to the formation of many free electrons in the conduction band and the escalation of adsorption sites on the delaminated MXene surface during photocatalysis [58]. Further increment in the dosage (2.0 g/L) has resulted in no Cr(VI) removal increment at equilibrium. In addition to increasing

Cr(VI) removal at equilibrium, an increase in delaminated MXene loading accelerated removal kinetics. The saturation of Cr(VI) removal efficiency at high photocatalyst loading could be explained by the excess binding sites of delaminated MXene for Cr(VI).

### *3.3.3. Effect of Cr(VI) concentration*

The initial concentration of Cr(VI) is another operating parameter in the adsorption and photocatalysis experiment because it increases an osmotic pressure that drives the adsorption of a metal ion to an adsorbent surface from an aqueous solution [56]. The effect of initial Cr(VI) concentration on its removal efficiency by the adsorption-assisted photocatalytic process was evaluated by varying the initial Cr(VI) concentration from 5 to 25 mg/L. The equilibrium time for Cr(VI) removal is longer as the initial Cr(VI) concentration increases. The removal efficiency of Cr(VI) decreased from 100% to 64.9%, with the increasing initial Cr(VI) concentration from 5 to 25 mg/L. High initial Cr(VI) concentration resulted in the saturation of vacant sites on delaminated MXene, causing a further extension of the reaction time for a little improvement to the pollutant removal [59,60]. Interestingly, even at a high concentration, the yellow colour of the initial Cr(VI) solution became more colourless after prolonging the reaction time, demonstrating the effectiveness of delaminated MXene on Cr(VI) removal. The effects of various operating parameters are displayed in Figure 7b-d.

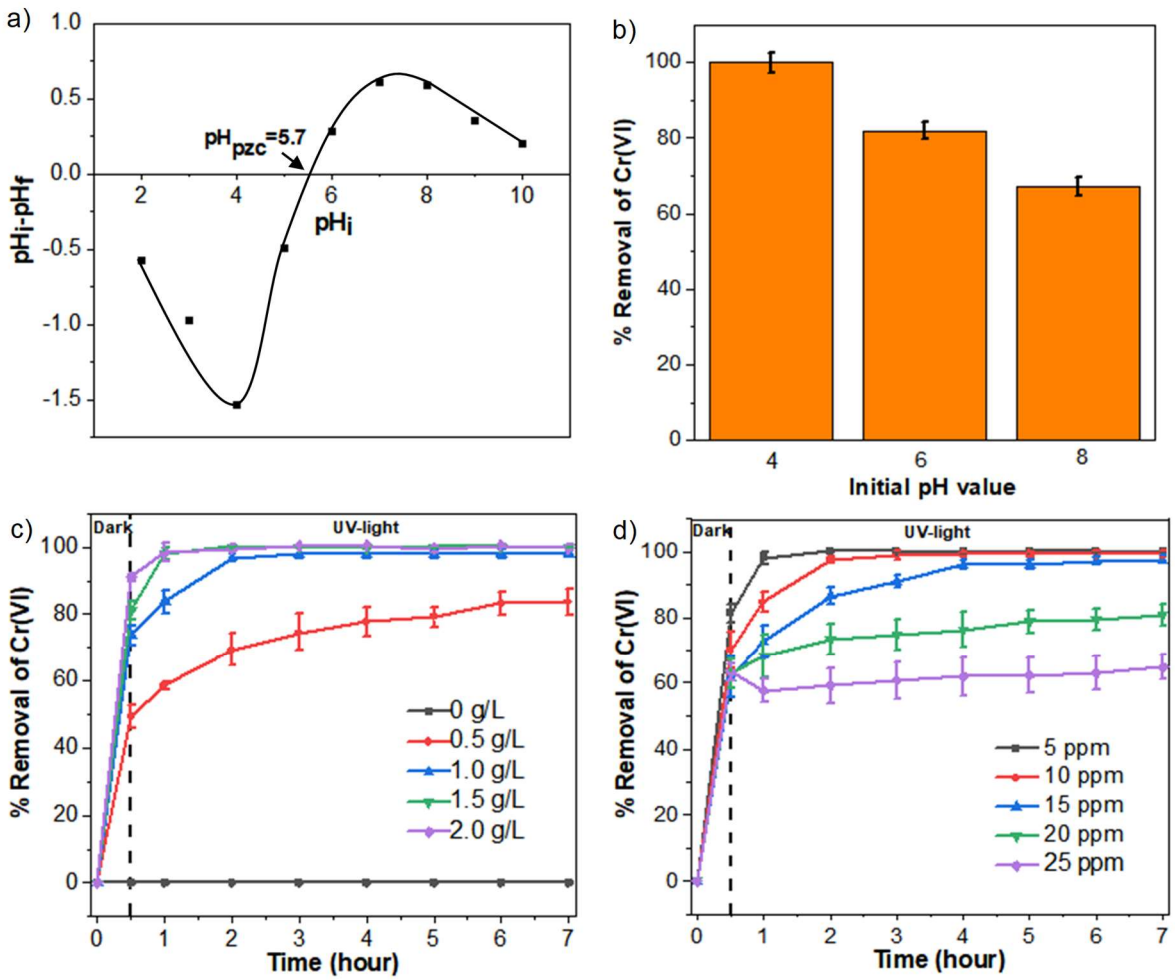


Figure 7. a) pHpzc of delaminated MXene, effect of various operating parameters on Cr(VI) removal at different b)pH value (catalyst dosage 1.5g/L, Cr(VI) concentration 5mg/L) c) photocatalyst dosage (Cr(VI) concentration 5mg/L ) and d) initial concentration of Cr(VI) (catalyst dosage 1.5g/L).

### *3.4. Isotherm and kinetic analysis*

The isotherm of Cr(VI) removal was calculated from the adsorption results. The isotherm was analysed using Freundlich and Langmuir isotherm models (Figure 8 (b and c)). The linear plot of the Langmuir model ($c_e$ versus $c_e/q_e$) gave a better agreement with experimental data than the Freundlich model. According to the Langmuir model, the Cr(VI) removal mechanism was attributed to the physical and monolayer adsorption [56,61]. Langmuir isotherm also suggests that the monolayer site energy of adsorption properties on the adsorbent surface is equal and saturated after the monolayer adsorption [62,63]. The values of the slope, linear constant and adsorption parameters are tabulated in Table 2. The

removal efficiency and qmax 6.28 mg/g) Cr(VI) obtained in this study is comparable to other reported adsorbents such as activated carbon, activated charcoal, graphene oxide, Zn-graphene oxide and iron. This proved that MXene synthesized in this study demonstrated a potential adsorbent for Cr(VI) removal. Table 1 presents a comparison of the adsorption capacity of different adsorbents at specific pH values.

Table 1. Adsorption capacities of Cr(VI) by different adsorbents.

| Adsorbent | pH | qmax (mg/g) | References |
|---|---|---|---|
| Graphene oxide | 4 | 1.22 | [64] |
| Iron | 4 | 1.27 | [65] |
| Zinc-Graphene oxide | 4 | 3.67 | [66] |
| Titanium dioxide | 3 | 23.8 | [67] |
| Activated alumina | 2 | 7.44 | [68] |
| Delaminated MXene | 4 | 6.25 | Present work |

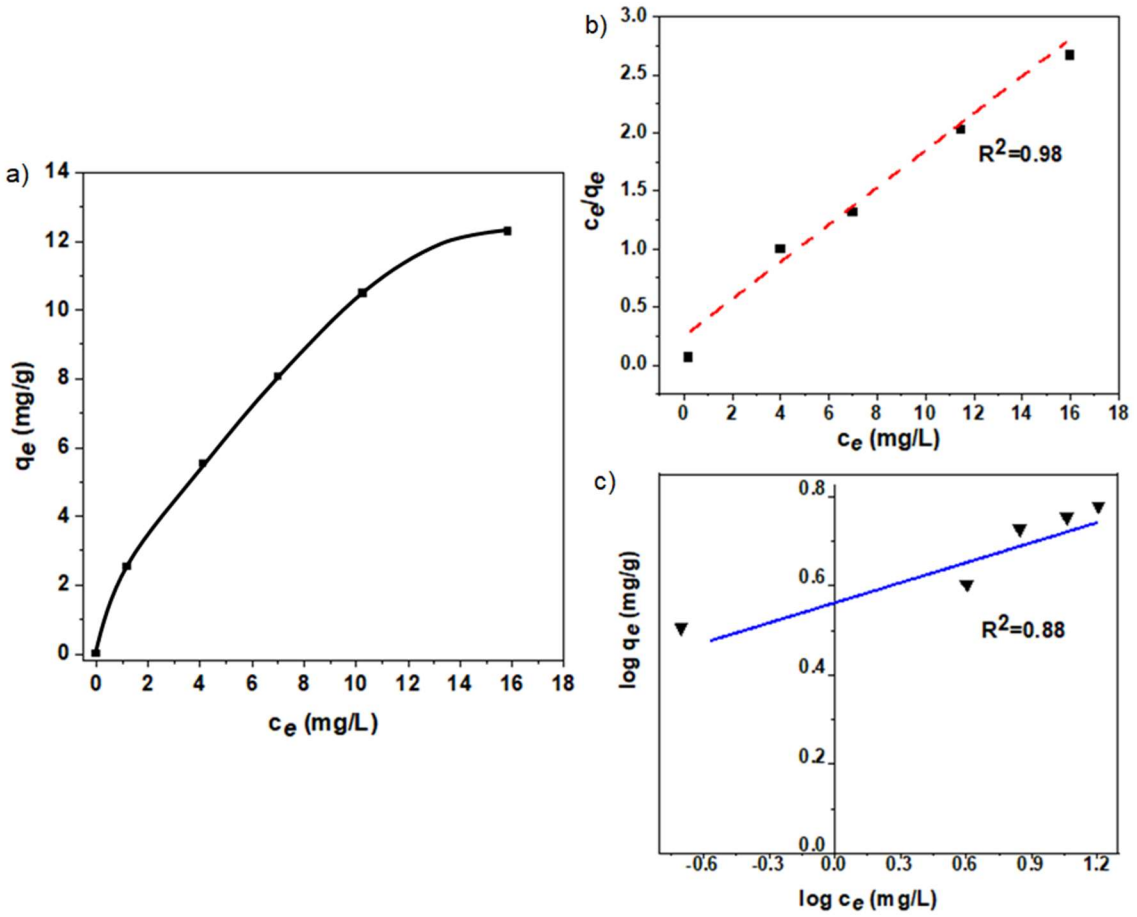


Figure 8. (a) ce versus qe plot, (b) Langmuir isotherm model, and (c) Freundlich isotherm model for Cr(VI) removal at different concentrations via adsorption under dark conditions.

The kinetics of the adsorption process was analyzed using pseudo-first- and pseudo-second order models. Figure 9 shows the pseudo-first- and pseudo-second-order models for Cr(VI) removal. The pseudo-second-order model displayed a better agreement than the pseudo-first-order model. This result suggests that the removal of Cr(VI) were controlled by the chemisorption process involving the electrons exchange that provides a fast adsorption rate of pollutant [56,62,69]. Several works also reported the same findings on the removal of Cr(VI) onto different types of adsorbent/photocatalyst such as chitosan/g-$C_3N_4$/$TiO_2$ [62] and graphene/g-$C_3N_4$ [70]. The coefficients from kinetic models are summarised in Table 3.

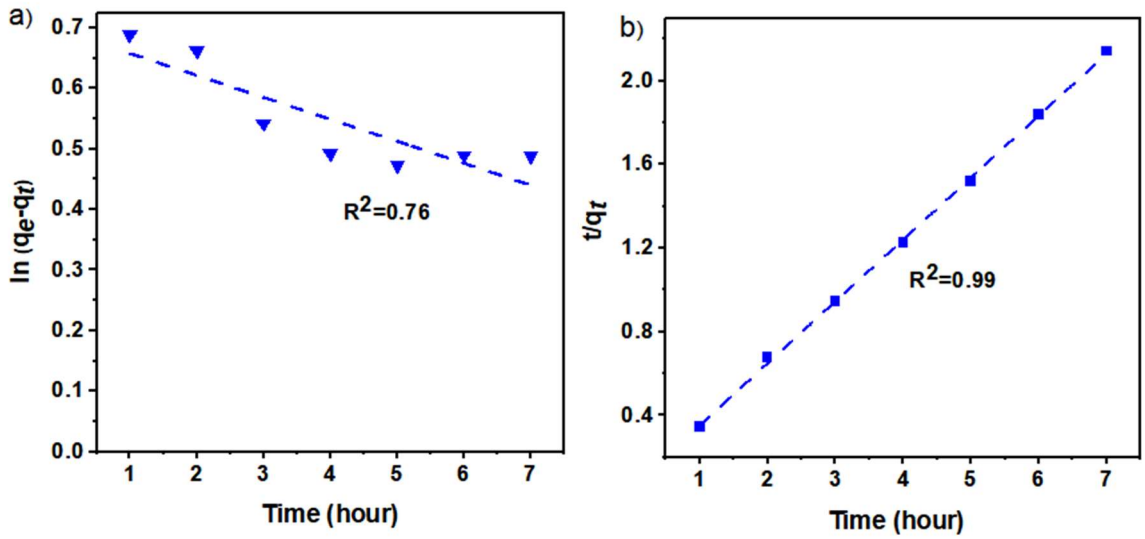


Figure 9. (a) Pseudo-first-order and (b) pseudo-second-order kinetic plots for Cr(VI) removal via adsorption

Table 2. Calculated parameters of Langmuir and Freundlich isotherm models.

| **Langmuir isotherm** | | **Freundlich isotherm** | |
|---|---|---|---|
| $K_L$ (L/mg) | 0.8744 | $K_F$ (mg/g)(L/mg)$^{(1/n)}$ | 3.8646 |
| $q_{max}$ (mg/g) | 6.2841 | $1/n$ | 0.1426 |
| $R^2$ | 0.9848 | $R^2$ | 0.8824 |

Table 3. Pseudo-first-order and pseudo-second-order kinetic parameters.

| **Pseudo-first-order model** | | | **Pseudo-second-order model** | | |
|---|---|---|---|---|---|
| $k_1$ ($min^{-1}$) | $R^2$ | $q_e$ (mg/g) | $k_2$ (g/mg·min) | $R^2$ | $q_e$ (mg/g) |
| −0.000001 | 0.7595 | 2.00031 | 0.00042 | 0.9999 | 204.082 |

### *3.5. Proposed mechanism for Cr(VI) removal*

Based on the overall results obtained, a possible mechanism of adsorptive–photocatalysis of Cr(VI) removal was proposed as schematically illustrated in Scheme 3. As the pH of Cr(VI) is less than pHpzc value=5.7, the C=O and OH− on delaminated MXene surface protonate with $H^{+,}$ forming a positively charged surface which attracts the negatively charged Cr(VI) via electrostatic interaction mechanism. On the other hand, at a pH range of 2 to 6, Cr(VI) mainly exists as $HCrO_4^-$ which can enhance the electrostatic attraction between Cr(VI) anions and the positively charged surface of the adsorbent. The subsequent mechanism under UV irradiation can be well described by photocatalytic reduction. Under UV light irradiation, when the energy of photons is higher or similar to the delaminated MXene bandgap energy, the electrons of delaminated MXene transfer from the valence band (VB) to the conduction band (CB), forming electron-hole pairs ($e^- - h^+$)(Eq.7). The electron-hole pairs further react with the available groups in water to generate oxygen and hydrogen ions, which could participate in the Cr(VI) removal (Eq.8). Meanwhile, Cr(VI) ions serve as the photoelectron acceptor and would react with the photogenerated electrons of delaminated MXene and reduce Cr(VI) to Cr(III) effectively. The Cr(VI) reduction process at (pH = 4-6) in this study can be expressed by the following equations [62]:

$$Ti_3C_2T_x + hv + 3e^- \rightarrow h^+ + e^- \quad (7)$$

$$2H_2O + 4H^+ + 3e^- \rightarrow O_2 + 4H^+ \quad (8)$$

$$HCrO_4^- + 7H^+ + 3e^- \rightarrow Cr^{3+} + 4H_2O \quad (9)$$

$$Cr_2O_7^{2-} + 14H^+ + 6e^- \rightarrow 2Cr^{3+} + 7H_2O \quad (10)$$

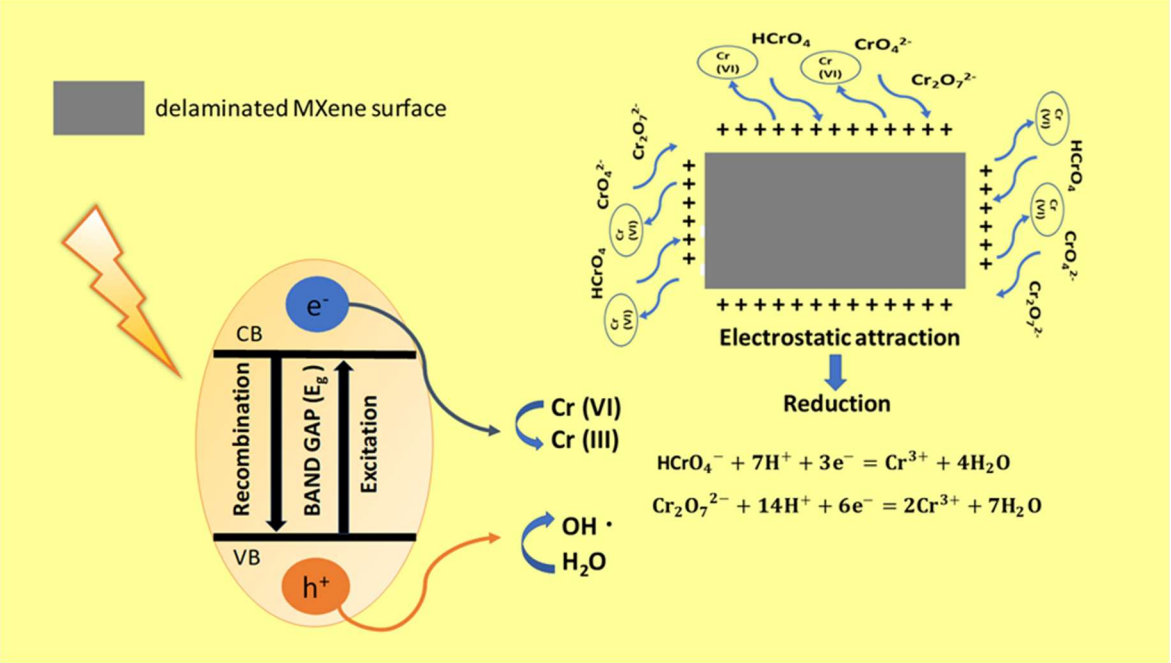


Scheme 3. Schematic illustration of proposed adsorption and photocatalytic mechanisms of Cr(VI) removal.

The mechanism of adsorption coupled with photocatalytic reduction can be proved by detecting the efficient reduction of Cr(VI) to Cr(III). Whereas AAS detect the amount of Cr(VI) regardless of their change in oxidation state, ultraviolet-visible (UV-Vis) spectrophotometer specifically detect Cr(VI) as it has significant UV absorbance at 543nm. Cr(III) concentration was calculated by subtracting the Cr(VI) concentration using UV-Vis spectrophotometer from the total Cr based on AAS measurement. The detailed trend of Cr(VI) reduction to Cr(III) can be seen in Figure 9a. Hence, the removal rate of Cr(VI) increased rapidly after placing the Cr(VI) solution under UV light irradiation. To further confirm the reduction of Cr(VI), XPS spectrum of Cr 2p after the reaction was analyzed (Figure 9b). Two main peaks originating from Cr $2p_{3/2}$ and Cr $2p_{1/2}$ orbitals revealed binding energy bands occurring at around 576.85, 587.34 and 578.65, 586.94, which can be assigned to the higher oxidation state of Cr, Cr(VI) and lower oxidation state of Cr, Cr(III), respectively [71].

Moreover, the XPS spectra of delaminated MXene were compared to the fresh delaminated MXene to investigate the change of the chemical state of delaminated MXene after Cr(VI) removal as shown in Figure 10, the binding energy of Ti2p of $TiO_2$ shifts from (459.18) to a lower value (458.80) illustrating that the proportion of Ti3+ becomes larger.

This observation indicates that delaminated MXene $Ti_3C_2T_x$ particles react in Cr(VI) solution and form $TiO_2$ on its surface, decreasing the $Ti_3C_2$ signal. The XPS spectrum can be verified in C 1s and O 1s regions. The high peak of C-O after reaction showed binding of Ti-C reduced to C-O. The oxidation of $Ti_3C_2T_x$ into Ti oxides is plausibly due to the interaction between $Ti_3C_2T_x$, Cr(VI), water (H2O) and Oxygen(O2). As a result, the oxidation of $Ti_3C_2T_x$ layers into nanoscale $TiO_2$ may lead to an increase in the accessible surface area, which could explain the increase in Cr(VI) removal and reduction, especially under light irradiation. However, further research is needed to focus on the stability of MXene in an aqueous solution over a certain period.

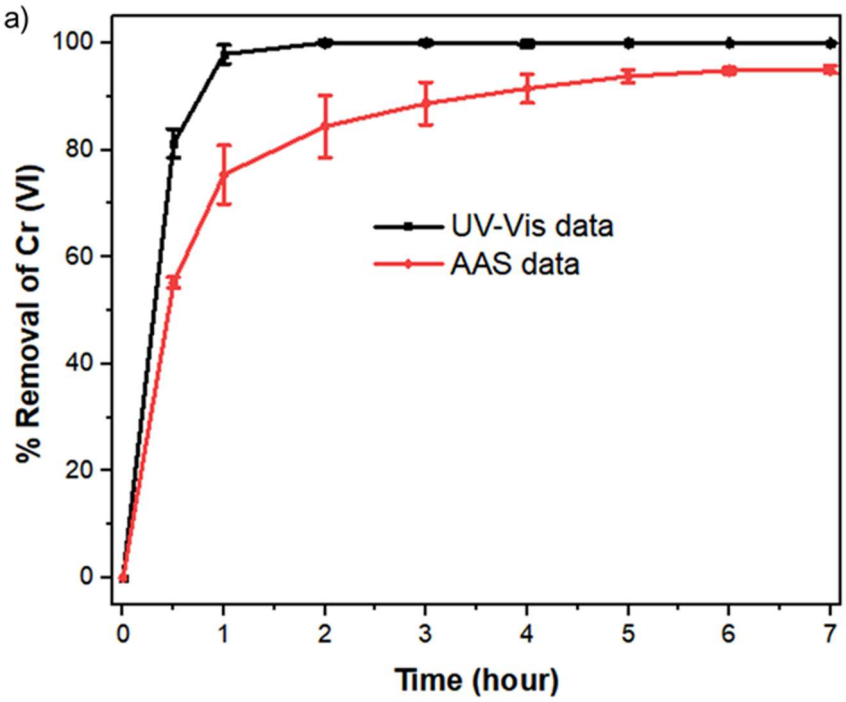

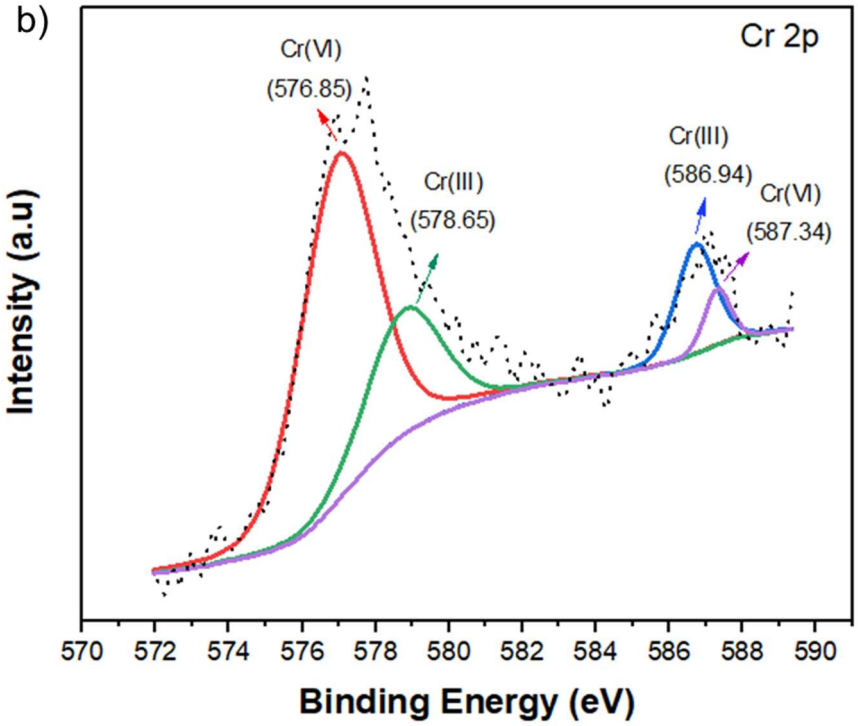


Figure 10. a) Removal efficiency of total Cr and Cr(VI) using AAS and UV-Vis spectroscopy b) XPS spectra of Cr 2p peak on delaminated MXene after adsorption-assisted photocatalysis process

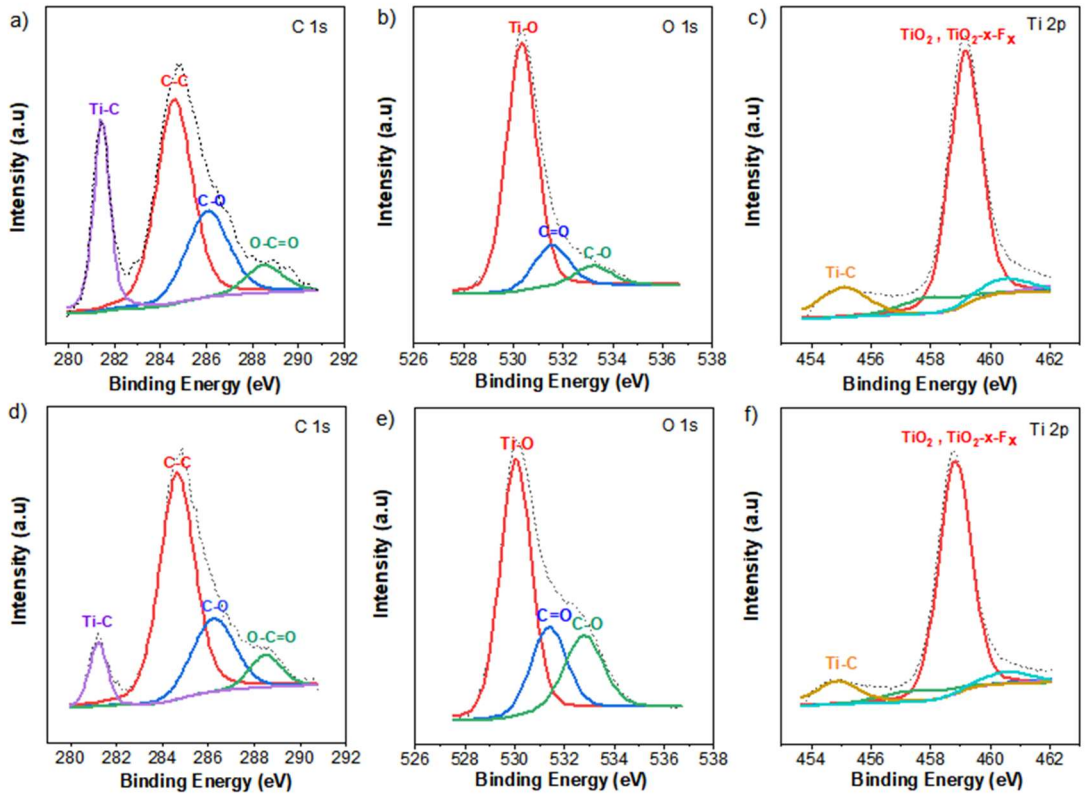


Figure 11. XPS spectra of a-c) delaminated MXene d-e) delaminated MXene after reaction

## 4.0 Conclusion

This work successfully synthesized delaminated MXene by etching the MAX phase of $Ti_3AlC_2$ and characterized using EDX, XRD, FTIR, FESEM, BET, TGA, UV-VIS-NIR and XPS analysis. The Cr(VI) removal of the delaminated MXene via adsorption-assisted photocatalysis was investigated by evaluating the effect of pH, delaminated MXene dosage, and initial concentration of Cr(VI). The optimum pH value for high Cr(VI) removal from aqueous solution was at pH 4. Experimental work demonstrated that the best photocatalyst dosage and initial Cr(VI) concentration were 1.5 g/L and 5 mg/L, respectively. The Cr(VI) removal reached 100% under UV light irradiation only within 3 hour reaction time, whereas simple adsorption gave approximately 96.9% removal after 7 hour. Overall, the photocatalytic process exhibited approximately 28.9% higher Cr(VI) removal efficiency than adsorption. Such excellent performance was attributed to the synergistic effect of electrostatic attraction of delaminated MXene surface with Cr(VI) ions and photogenerated CB electrons in delaminated MXene under UV- light irradiation. The Langmuir model provided the best fit to the equilibrium isotherm, confirming that the adsorption of Cr(VI) was due to the monolayer sorption processes. The pseudo-second-order kinetic model further described the time dependence on Cr(VI) sorption. The detailed mechanism for adsorption-assisted photocatalysis of Cr(VI) by delaminated MXene was proposed and demonstrated that delaminated MXene has potential as an excellent photocatalytic adsorbent for removing Cr(VI) from an aqueous solution.

**Acknowledgements**

The authors gratefully acknowledged the Ministry of Higher Education Malaysia (MOHE) for the FRGS research funding (600-IRMI/FRGS 5/3 (441/2019)). NSJ would also like to thank the Advanced Membrane Technology Research Centre (AMTEC), Universiti Teknologi Malaysia (UTM), Malaysia, for the awarded AMTEC fellowship.

Conflicts of Interest: The authors declare no conflict of interest.

## References


[1] H. Li, N. Li, P. Zuo, S. Qu, W. Shen, Efficient adsorption-reduction synergistic effects of sulfur, nitrogen and oxygen heteroatom co-doped porous carbon spheres for chromium(VI) removal, Colloids and Surfaces A: Physicochemical and Engineering Aspects. 618 (2021) 126502. doi:10.1016/j.colsurfa.2021.126502.

[2] R.F.S. Barbosa, A.G. Souza, H.F. Maltez, D.S. Rosa, Chromium removal from contaminated wastewaters using biodegradable membranes containing cellulose nanostructures, Chemical Engineering Journal. 395 (2020) 125055. doi:10.1016/j.cej.2020.125055.

[3] V.T. Trang, L.T. Tam, N. Van Quy, V.N. Phan, H. Van Tuan, T.Q. Huy, N.X. Dinh, A.T. Le, Enhanced adsorption efficiency of inorganic chromium (VI) ions by using carbon-encapsulated hematite nanocubes, Journal of Science: Advanced Materials and Devices. 5 (2020) 392–399. doi:10.1016/j.jsamd.2020.05.007.

[4] H. Liang, B. Song, P. Peng, G. Jiao, X. Yan, D. She, Preparation of three-dimensional honeycomb carbon materials and their adsorption of Cr(VI), Chemical Engineering Journal. 367 (2019) 9–16. doi:10.1016/j.cej.2019.02.121.

[5] J. Zhou, Y. Wang, J. Wang, W. Qiao, D. Long, L. Ling, Effective removal of hexavalent chromium from aqueous solutions by adsorption on mesoporous carbon microspheres, Journal of Colloid and Interface Science. 462 (2016) 200–207. doi:10.1016/j.jcis.2015.10.001.

[6] Y. Tadjenant, N. Dokhan, A. Barras, A. Addad, R. Jijie, S. Szunerits, R. Boukherroub, Graphene oxide chemically reduced and functionalized with KOH-PEI for efficient Cr(VI) adsorption and reduction in acidic medium, Chemosphere. 258 (2020) 127316. doi:10.1016/j.chemosphere.2020.127316.

[7] G. Chen, H. Liu, Photochemical removal of hexavalent chromium and nitrate from ion-exchange brine waste using carbon-centered radicals, Chemical Engineering Journal. 396 (2020) 125136. doi:10.1016/j.cej.2020.125136.

[8] Y. Xie, J. Lin, J. Liang, M. Li, Y. Fu, H. Wang, S. Tu, J. Li, Hypercrosslinked mesoporous poly(ionic liquid)s with high density of ion pairs: Efficient adsorbents for Cr(VI) removal via ion-exchange, Chemical Engineering Journal. 378 (2019) 122107. doi:10.1016/j.cej.2019.122107.

[9] B. Xie, C. Shan, Z. Xu, X. Li, X. Zhang, J. Chen, B. Pan, One-step removal of Cr(VI) at alkaline pH by UV/sulfite process: Reduction to Cr(III) and in situ Cr(III) precipitation, Chemical Engineering Journal. 308 (2017) 791–797. doi:10.1016/j.cej.2016.09.123.

[10] S. Koushkbaghi, A. Zakialamdari, M. Pishnamazi, H.F. Ramandi, M. Aliabadi, M. Irani, Aminated-Fe3O4 nanoparticles filled chitosan/PVA/PES dual layers nanofibrous membrane for the removal of Cr(VI) and Pb(II) ions from aqueous solutions in adsorption and membrane processes, Chemical Engineering Journal. 337 (2018) 169–182. doi:10.1016/j.cej.2017.12.075.

[11] H. Semghouni, S. Bey, A. Figoli, A. Criscuoli, M. Benamor, E. Drioli, Chromium

(VI) removal by Aliquat-336 in a novel multiframe flat sheet membrane contactor, Chemical Engineering and Processing - Process Intensification. 147 (2020) 107765. doi:10.1016/j.cep.2019.107765.

[12] S. Zhao, Z. Chen, J. Shen, Y. Qu, B. Wang, X. Wang, Enhanced Cr(VI) removal based on reduction-coagulation-precipitation by NaBH4 combined with fly ash leachate as a catalyst, Chemical Engineering Journal. 322 (2017) 646–656. doi:10.1016/j.cej.2017.04.057.

[13] L. Xiang, C.G. Niu, N. Tang, X.X. Lv, H. Guo, Z.W. Li, H.Y. Liu, L.S. Lin, Y.Y. Yang, C. Liang, Polypyrrole coated molybdenum disulfide composites as adsorbent for enhanced removal of Cr(VI) in aqueous solutions by adsorption combined with reduction, Chemical Engineering Journal. 408 (2021) 127281. doi:10.1016/j.cej.2020.127281.

[14] J. Sun, Y. Hou, Z. Yu, L. Tu, Y. Yan, S. Qin, S. Chen, D. Lan, H. Zhu, S. Wang, Visible-light-driven Z-scheme Zn3In2S6/AgBr photocatalyst for boosting simultaneous Cr (VI) reduction and metronidazole oxidation: Kinetics, degradation pathways and mechanism, Journal of Hazardous Materials. (2021) 126543. doi:10.1016/j.jhazmat.2021.126543.

[15] Y. Liu, D. Yang, T. Xu, Y. Shi, L. Song, Z.Z. Yu, Continuous photocatalytic removal of chromium (VI) with structurally stable and porous Ag/Ag3PO4/reduced graphene oxide microspheres, Chemical Engineering Journal. 379 (2020) 122200. doi:10.1016/j.cej.2019.122200.

[16] D. Lu, P. Fang, W. Wu, J. Ding, L. Jiang, X. Zhao, C. Li, M. Yang, Y. Li, D. Wang, Solvothermal-assisted synthesis of self-assembling TiO2 nanorods on large graphitic carbon nitride sheets with their anti-recombination in the photocatalytic removal of Cr(VI) and rhodamine B under VIsible light irradiation, Nanoscale. 9 (2017) 3231–3245. doi:10.1039/c6nr09137g.

[17] L.W. Duresa, D.H. Kuo, K.E. Ahmed, M.A. Zeleke, H. Abdullah, Highly enhanced photocatalytic Cr(vi) reduction using In-doped Zn(O,S) nanoparticles, New Journal of Chemistry. 43 (2019) 8746–8754. doi:10.1039/c9nj01511f.

[18] Y. Yang, L. Yan, J. Li, J. Li, T. Yan, M. Sun, Z. Pei, Synergistic adsorption and photocatalytic reduction of Cr(VI) using Zn-Al-layered double hydroxide and TiO2 composites, Applied Surface Science. 492 (2019) 487–496. doi:10.1016/j.apsusc.2019.06.229.

[19] Q. Xia, B. Huang, X. Yuan, H. Wang, Z. Wu, L. Jiang, T. Xiong, J. Zhang, G. Zeng, H. Wang, Modified stannous sulfide nanoparticles with metal-organic framework: Toward efficient and enhanced photocatalytic reduction of chromium (VI) under visible light, Journal of Colloid and Interface Science. 530 (2018) 481–492. doi:10.1016/j.jcis.2018.05.015.

[20] C.R. Chen, H.Y. Zeng, S. Xu, J.C. Shen, G. Hu, R.L. Zhu, J.Z. Du, Y.X. Sun, Facile fabrication of CdS/ZnAlO heterojunction with enhanced photocatalytic activity for Cr(VI) reduction under visible light, Applied Clay Science. 165 (2018) 197–204. doi:10.1016/j.clay.2018.08.019.

[21] Z. Chen, Y. Luo, C. Huang, X. Shen, In situ assembly of ZnO/graphene oxide on synthetic molecular receptors: Towards selective photoreduction of Cr(VI) via interfacial synergistic catalysis, Chemical Engineering Journal. 414 (2021) 128914. doi:10.1016/j.cej.2021.128914.

[22] Y. Sun, L. Xu, P. Jin, X. Bai, X. Jin, X. Shi, Simultaneous removal of colorless micropollutants and hexavalent chromium by pristine TiO2 under visible light: An electron transfer mechanism, Chemical Engineering Journal. 405 (2021) 126968. doi:10.1016/j.cej.2020.126968.

[23] L. Hou, Y. Zhang, Y. Ma, Y. Wang, Z. Hu, Y. Gao, Z. Han, Reduced Phosphomolybdate Hybrids as Efficient Visible-Light Photocatalysts for Cr(VI) Reduction, Inorganic Chemistry. 58 (2019) 16667–16675. doi:10.1021/acs.inorgchem.9b02777.

[24] M. Naguib, M. Kurtoglu, V. Presser, J. Lu, J. Niu, M. Heon, L. Hultman, Y. Gogotsi, M.W. Barsoum, Two-Dimensional Nanocrystals Produced by Exfoliation of Ti3AlC2, Advanced Materials. 23 (2011) 4248–4253. doi:10.1002/adma.201102306.

[25] M. Alhabeb, K. Maleski, B. Anasori, P. Lelyukh, L. Clark, S. Sin, Y. Gogotsi, Guidelines for Synthesis and Processing of Two-Dimensional Titanium Carbide (Ti3C2Tx MXene), Chemistry of Materials. 29 (2017) 7633–7644. doi:10.1021/acs.chemmater.7b02847.

[26] J. Lao, R. Lv, J. Gao, A. Wang, J. Wu, J. Luo, Aqueous Stable Ti 3 C 2 MXene Membrane with Fast and Photoswitchable Nanofluidic Transport, ACS Nano. 12 (2018) 12464–12471. doi:10.1021/acsnano.8b06708.

[27] S. Kim, M. Yu, Y. Yoon, Fouling and Retention Mechanisms of Selected Cationic and Anionic Dyes in a Ti3C2Tx MXene-Ultrafiltration Hybrid System, ACS Applied Materials and Interfaces. 12 (2020) 16557–16565. doi:10.1021/acsami.0c02454.

[28] B. Zielińska, A. Wróblewska, K. Maślana, P. Miądlicki, K. Kiełbasa, A. Rozmysłowska-Wojciechowska, M. Petrus, J. Woźniak, A.M. Jastrzębska, B. Michalkiewicz, E. Mijowska, High catalytic performance of 2D Ti3C2Tx MXene in α-pinene isomerization to camphene, Applied Catalysis A: General. 604 (2020) 117765. doi:10.1016/j.apcata.2020.117765.

[29] V. Sharma, A. Kumar, A. Kumar, V. Krishnan, Enhanced photocatalytic activity of two dimensional ternary nanocomposites of ZnO–Bi2WO6–Ti3C2 MXene under natural sunlight irradiation, Chemosphere. 287 (2022). doi:10.1016/J.CHEMOSPHERE.2021.132119.

[30] X. Feng, Z. Yu, Y. Sun, R. Long, M. Shan, X. Li, Y. Liu, J. Liu, Review MXenes as a new type of nanomaterial for environmental applications in the photocatalytic degradation of water pollutants, Ceramics International. (2020). doi:10.1016/j.ceramint.2020.11.151.

[31] C. Prasad, X. Yang, Q. Liu, H. Tang, A. Rammohan, S. Zulfiqar, G. V. Zyryanov,

S. Shah, Recent advances in MXenes supported semiconductors based photocatalysts: Properties, synthesis and photocatalytic applications, Journal of Industrial and Engineering Chemistry. 85 (2020) 1–33. doi:10.1016/j.jiec.2019.12.003.

[32] B. Sun, P. Qiu, Z. Liang, Y. Xue, X. Zhang, L. Yang, H. Cui, J. Tian, The fabrication of 1D/2D CdS nanorod@Ti3C2 MXene composites for good photocatalytic activity of hydrogen generation and ammonia synthesis, Chemical Engineering Journal. 406 (2021) 127177. doi:10.1016/j.cej.2020.127177.

[33] Y. Ying, Y. Liu, X. Wang, Y. Mao, W. Cao, P. Hu, X. Peng, Two-dimensional titanium carbide for efficiently reductive removal of highly toxic chromium(VI) from water, ACS Applied Materials and Interfaces. 7 (2015) 1795–1803. doi:10.1021/am5074722.

[34] Z. Li, Y. Wu, 2D Early Transition Metal Carbides (MXenes) for Catalysis, Small. 15 (2019) 1804736. doi:10.1002/SMLL.201804736.

[35] H. Wang, Y. Sun, Y. Wu, W. Tu, S. Wu, X. Yuan, G. Zeng, Z.J. Xu, S. Li, J.W. Chew, Electrical promotion of spatially photoinduced charge separation via interfacial-built-in quasi-alloying effect in hierarchical Zn2In2S5/Ti3C2(O, OH)x hybrids toward efficient photocatalytic hydrogen evolution and environmental remediation, Applied Catalysis B: Environmental. 245 (2019) 290–301. doi:10.1016/j.apcatb.2018.12.051.

[36] A. Shahzad, K. Rasool, W. Miran, M. Nawaz, J. Jang, K.A. Mahmoud, D.S. Lee, Two-Dimensional Ti3C2Tx MXene Nanosheets for Efficient Copper Removal from Water, ACS Sustainable Chemistry and Engineering. 5 (2017) 11481–11488. doi:10.1021/acssuschemeng.7b02695.

[37] Q. Peng, J. Guo, Q. Zhang, J. Xiang, B. Liu, A. Zhou, R. Liu, Y. Tian, Unique lead adsorption behavior of activated hydroxyl group in two-dimensional titanium carbide, Journal of the American Chemical Society. 136 (2014) 4113–4116. doi:10.1021/ja500506k.

[38] A. Shahzad, K. Rasool, W. Miran, M. Nawaz, J. Jang, K.A. Mahmoud, D.S. Lee, Mercuric ion capturing by recoverable titanium carbide magnetic nanocomposite, Journal of Hazardous Materials. 344 (2018) 811–818. doi:10.1016/j.jhazmat.2017.11.026.

[39] K. Fu, X. Liu, D. Yu, J. Luo, Z. Wang, J.C. Crittenden, Highly Efficient and Selective Hg(II) Removal from Water Using Multilayered Ti3C2O xMXene via Adsorption Coupled with Catalytic Reduction Mechanism, Environmental Science and Technology. 54 (2020) 16212–16220. doi:10.1021/acs.est.0c05532.

[40] P. Karthikeyan, K. Ramkumar, K. Pandi, A. Fayyaz, S. Meenakshi, C.M. Park, Effective removal of Cr(VI) and methyl orange from the aqueous environment using two-dimensional (2D) Ti3C2Tx MXene nanosheets, Ceramics International. 47 (2021) 3692–3698. doi:10.1016/J.CERAMINT.2020.09.221.

[41] Y. Tang, C. Yang, W. Que, A novel two-dimensional accordion-like titanium

carbide (MXene) for adsorption of Cr(VI) from aqueous solution, Journal of Advanced Dielectrics. 8 (2018) 1850035. doi:10.1142/S2010135X18500352.

[42] A. Kong, Y. Sun, M. Peng, H. Gu, Y. Fu, J. Zhang, W. Li, Amino-functionalized MXenes for efficient removal of Cr(VI), Colloids and Surfaces A: Physicochemical and Engineering Aspects. 617 (2021) 126388. doi:10.1016/j.colsurfa.2021.126388.

[43] O. Mashtalir, K.M. Cook, V.N. Mochalin, M. Crowe, M.W. Barsoum, Y. Gogotsi, Dye adsorption and decomposition on two-dimensional titanium carbide in aqueous media, Journal of Materials Chemistry A. 2 (2014) 14334–14338. doi:10.1039/C4TA02638A.

[44] M. Rosales, A. Garcia, V.M. Fuenzalida, R. Espinoza-González, G. Song, B. Wang, J. Yu, F. Gracia, A. Rosenkranz, Unprecedented arsenic photo-oxidation behavior of few- and multi-layer Ti3C2Tx nano-sheets, Applied Materials Today. 20 (2020) 100769. doi:10.1016/j.apmt.2020.100769.

[45] D. Zhao, C. Cai, Preparation of Bi2MoO6/Ti3C2MXene heterojunction photocatalysts for fast tetracycline degradation and Cr(vi) reduction, Inorganic Chemistry Frontiers. 7 (2020) 2799–2808. doi:10.1039/d0qi00540a.

[46] N.H. Alias, J. Jaafar, S. Samitsu, N. Yusof, M.H.D. Othman, M.A. Rahman, A.F. Ismail, F. Aziz, W.N.W. Salleh, N.H. Othman, Photocatalytic degradation of oilfield produced water using graphitic carbon nitride embedded in electrospun polyacrylonitrile nanofibers, Chemosphere. 204 (2018) 79–86. doi:10.1016/j.chemosphere.2018.04.033.

[47] A. Lace, D. Ryan, M. Bowkett, J. Cleary, Chromium Monitoring in Water by Colorimetry Using Optimised 1,5-Diphenylcarbazide Method, International Journal of Environmental Research and Public Health. 16 (2019). doi:10.3390/IJERPH16101803.

[48] C. Peng, P. Wei, X. Chen, Y. Zhang, F. Zhu, Y. Cao, H. Wang, H. Yu, F. Peng, A hydrothermal etching route to synthesis of 2D MXene (Ti3C2, Nb2C): Enhanced exfoliation and improved adsorption performance, Ceramics International. 44 (2018) 18886–18893. doi:10.1016/j.ceramint.2018.07.124.

[49] G.P. Lim, C.F. Soon, M. Morsin, M.K. Ahmad, N. Nayan, K.S. Tee, Synthesis, characterization and antifungal property of Ti3C2Tx MXene nanosheets, Ceramics International. 46 (2020) 20306–20312. doi:10.1016/j.ceramint.2020.05.118.

[50] W. Feng, H. Luo, Y. Wang, S. Zeng, L. Deng, X. Zhou, H. Zhang, S. Peng, Ti3C2 MXene: A promising microwave absorbing material, RSC Advances. 8 (2018) 2398–2403. doi:10.1039/c7ra12616f.

[51] X. Gao, Z.K. Li, J. Xue, Y. Qian, L.Z. Zhang, J. Caro, H. Wang, Titanium carbide Ti3C2Tx (MXene) enhanced PAN nanofiber membrane for air purification, Journal of Membrane Science. 586 (2019) 162–169. doi:10.1016/j.memsci.2019.05.058.

[52] J. Chen, X. Yuan, F. Lyu, Q. Zhong, H. Hu, Q. Pan, Q. Zhang, Integrating MXene nanosheets with cobalt-tipped carbon nanotubes for an efficient oxygen reduction reaction, Journal of Materials Chemistry A. 7 (2019) 1281–1286.

doi:10.1039/c8ta10574j.

[53] J. Zhu, Y. Tang, C. Yang, F. Wang, M. Cao, Composites of TiO 2 Nanoparticles Deposited on Ti 3 C 2 MXene Nanosheets with Enhanced Electrochemical Performance , Journal of The Electrochemical Society. 163 (2016) A785–A791. doi:10.1149/2.0981605jes.

[54] L. Wang, B. Shi, Hydroxide conduction enhancement of chitosan membranes by functionalized MXene, Materials. 11 (2018). doi:10.3390/ma11112335.

[55] S. Alekseev, D. Korytko, M. Iazykov, S. Khainakov, V. Lysenko, Electrochemical Synthesis of Carbon Fluorooxide Nanoparticles from 3C-SiC Substrates, Journal of Physical Chemistry C. 119 (2015) 20503–20514. doi:10.1021/acs.jpcc.5b06524.

[56] U. Khalil, M.B. Shakoor, S. Ali, S.R. Ahmad, M. Rizwan, A.A. Alsahli, M.N. Alyemeni, Selective removal of hexavalent chromium from wastewater by rice husk: Kinetic, isotherm and spectroscopic investigation, Water (Switzerland). 13 (2021) 263. doi:10.3390/w13030263.

[57] T.D. Ntuli, T.H. Mongwe, L.L. Sikeyi, O. Mkhari, N.J. Coville, E.N. Nxumalo, M.S. Maubane-Nkadimeng, Removal of hexavalent chromium via an adsorption coupled reduction mechanism using olive oil derived carbon nano-onions, Environmental Nanotechnology, Monitoring and Management. 16 (2021) 100477. doi:10.1016/j.enmm.2021.100477.

[58] M. Shirzad-Siboni, M. Farrokhi, R. Darvishi Cheshmeh Soltani, A. Khataee, S. Tajassosi, Photocatalytic reduction of hexavalent chromium over ZnO nanorods immobilized on kaolin, Industrial and Engineering Chemistry Research. 53 (2014) 1079–1087. doi:10.1021/ie4032583.

[59] D. Jiang, Y. Yang, C. Huang, M. Huang, J. Chen, T. Rao, X. Ran, Removal of the heavy metal ion nickel (II) via an adsorption method using flower globular magnesium hydroxide, Journal of Hazardous Materials. 373 (2019) 131–140. doi:10.1016/j.jhazmat.2019.01.096.

[60] N.H. Mthombeni, S. Mbakop, S.C. Ray, T. Leswifi, A. Ochieng, M.S. Onyango, Highly efficient removal of chromium (VI) through adsorption and reduction: A column dynamic study using magnetized natural zeolite-polypyrrole composite, Journal of Environmental Chemical Engineering. 6 (2018) 4008–4017. doi:10.1016/j.jece.2018.05.038.

[61] A.L. Popovic, J.D. Rusmirovic, Z. Velickovic, T. Kovacevic, A. Jovanovic, I. Cvijetic, A.D. Marinkovic, Kinetics and column adsorption study of diclofenac and heavy-metal ions removal by amino-functionalized lignin microspheres, Journal of Industrial and Engineering Chemistry. 93 (2021) 302–314. doi:10.1016/j.jiec.2020.10.006.

[62] Q.H. Li, M. Dong, R. Li, Y.Q. Cui, G.X. Xie, X.X. Wang, Y.Z. Long, Enhancement of Cr(VI) removal efficiency via adsorption/photocatalysis synergy using electrospun chitosan/g-C3N4/TiO2 nanofibers, Carbohydrate Polymers. 253 (2021) 117200. doi:10.1016/j.carbpol.2020.117200.

[63] P.C. Okafor, C.O. Obadimu, Solar Photocatalytic Degradation of Phenol Using Cocos Nucifera (Coconut) Shells as Adsorbent, (2015). doi:10.15640/jcb.v3n1a3.

[64] N.K. Mondal, S. Chakraborty, Adsorption of Cr(VI) from aqueous solution on graphene oxide (GO) prepared from graphite: equilibrium, kinetic and thermodynamic studies, Applied Water Science. 10 (2020). doi:10.1007/S13201-020-1142-2.

[65] J. Bu, W. Li, N. Niu, N. Guo, H. Zhou, C. Chen, A. Ding, Adsorption of Cr(VI) from wastewater by iron-modified coconut shell biochar, E3S Web of Conferences. 248 (2021). doi:10.1051/E3SCONF/202124801059.

[66] S. Singh, A.G. Anil, S. Khasnabis, V. Kumar, B. Nath, V. Adiga, T.S.S. Kumar Naik, S. Subramanian, V. Kumar, J. Singh, P.C. Ramamurthy, Sustainable removal of Cr(VI) using graphene oxide-zinc oxide nanohybrid: Adsorption kinetics, isotherms and thermodynamics, Environmental Research. 203 (2022) 111891. doi:10.1016/J.ENVRES.2021.111891.

[67] M. Malakootian, F. Mansuri, Hexavalent chromium removal by titanium dioxide photocatalytic reduction and the effect of phenol and humic acid on its removal efficiency, International Journal of Environmental Health Engineering. 4 (2015) 19. doi:10.4103/2277-9183.157720.

[68] S. Mor, K. Ravindra, N.R. Bishnoi, Adsorption of chromium from aqueous solution by activated alumina and activated charcoal, Bioresource Technology. 98 (2007) 954–957. doi:10.1016/J.BIORTECH.2006.03.018.

[69] I.-I.N. Etim, P.C. Okafor, R.A. Etiuma, C.O. Obadimu, Solar Photocatalytic Degradation of Phenol Using Cocos Nucifera (Coconut) Shells as Adsorbent, Journal of Chemistry and Biochemistry. 3 (2015). doi:10.15640/jcb.v3n1a3.

[70] X. Wang, Y. Liang, W. An, J. Hu, Y. Zhu, W. Cui, Removal of chromium (VI) by a self-regenerating and metal free g-C3N4/graphene hydrogel system via the synergy of adsorption and photo-catalysis under visible light, Applied Catalysis B: Environmental. 219 (2017) 53–62. doi:10.1016/j.apcatb.2017.07.008.

[71] A. Jain, A. Kumar, H. Kaur, V. Krishnan, Strategic combination of ultra violet-visible-near infrared light active materials towards maximum utilization of full solar spectrum for photocatalytic chromium reduction, Chemosphere. 267 (2021) 128884. doi:10.1016/J.CHEMOSPHERE.2020.128884.

[1] H. Li, N. Li, P. Zuo, S. Qu, W. Shen, Efficient adsorption-reduction synergistic effects of sulfur, nitrogen and oxygen heteroatom co-doped porous carbon spheres for chromium(VI) removal, Colloids and Surfaces A: Physicochemical and Engineering Aspects. 618 (2021) 126502. doi:10.1016/j.colsurfa.2021.126502.

[2] R.F.S. Barbosa, A.G. Souza, H.F. Maltez, D.S. Rosa, Chromium removal from contaminated wastewaters using biodegradable membranes containing cellulose

nanostructures, Chemical Engineering Journal. 395 (2020) 125055. doi:10.1016/j.cej.2020.125055.

[3] V.T. Trang, L.T. Tam, N. Van Quy, V.N. Phan, H. Van Tuan, T.Q. Huy, N.X. Dinh, A.T. Le, Enhanced adsorption efficiency of inorganic chromium (VI) ions by using carbon-encapsulated hematite nanocubes, Journal of Science: Advanced Materials and Devices. 5 (2020) 392–399. doi:10.1016/j.jsamd.2020.05.007.

[4] H. Liang, B. Song, P. Peng, G. Jiao, X. Yan, D. She, Preparation of three-dimensional honeycomb carbon materials and their adsorption of Cr(VI), Chemical Engineering Journal. 367 (2019) 9–16. doi:10.1016/j.cej.2019.02.121.

[5] J. Zhou, Y. Wang, J. Wang, W. Qiao, D. Long, L. Ling, Effective removal of hexavalent chromium from aqueous solutions by adsorption on mesoporous carbon microspheres, Journal of Colloid and Interface Science. 462 (2016) 200–207. doi:10.1016/j.jcis.2015.10.001.

[6] Y. Tadjenant, N. Dokhan, A. Barras, A. Addad, R. Jijie, S. Szunerits, R. Boukherroub, Graphene oxide chemically reduced and functionalized with KOH-PEI for efficient Cr(VI) adsorption and reduction in acidic medium, Chemosphere. 258 (2020) 127316. doi:10.1016/j.chemosphere.2020.127316.

[7] G. Chen, H. Liu, Photochemical removal of hexavalent chromium and nitrate from ion-exchange brine waste using carbon-centered radicals, Chemical Engineering Journal. 396 (2020) 125136. doi:10.1016/j.cej.2020.125136.

[8] Y. Xie, J. Lin, J. Liang, M. Li, Y. Fu, H. Wang, S. Tu, J. Li, Hypercrosslinked mesoporous poly(ionic liquid)s with high density of ion pairs: Efficient adsorbents for Cr(VI) removal via ion-exchange, Chemical Engineering Journal. 378 (2019) 122107. doi:10.1016/j.cej.2019.122107.

[9] B. Xie, C. Shan, Z. Xu, X. Li, X. Zhang, J. Chen, B. Pan, One-step removal of Cr(VI) at alkaline pH by UV/sulfite process: Reduction to Cr(III) and in situ Cr(III) precipitation, Chemical Engineering Journal. 308 (2017) 791–797. doi:10.1016/j.cej.2016.09.123.

[10] S. Koushkbaghi, A. Zakialamdari, M. Pishnamazi, H.F. Ramandi, M. Aliabadi, M. Irani, Aminated-Fe3O4 nanoparticles filled chitosan/PVA/PES dual layers nanofibrous membrane for the removal of Cr(VI) and Pb(II) ions from aqueous solutions in adsorption and membrane processes, Chemical Engineering Journal. 337 (2018) 169–182. doi:10.1016/j.cej.2017.12.075.

[11] H. Semghouni, S. Bey, A. Figoli, A. Criscuoli, M. Benamor, E. Drioli, Chromium

(VI) removal by Aliquat-336 in a novel multiframe flat sheet membrane contactor, Chemical Engineering and Processing - Process Intensification. 147 (2020) 107765. doi:10.1016/j.cep.2019.107765.

[12] S. Zhao, Z. Chen, J. Shen, Y. Qu, B. Wang, X. Wang, Enhanced Cr(VI) removal based on reduction-coagulation-precipitation by NaBH4 combined with fly ash leachate as a catalyst, Chemical Engineering Journal. 322 (2017) 646–656. doi:10.1016/j.cej.2017.04.057.

[13] L. Xiang, C.G. Niu, N. Tang, X.X. Lv, H. Guo, Z.W. Li, H.Y. Liu, L.S. Lin, Y.Y. Yang, C. Liang, Polypyrrole coated molybdenum disulfide composites as adsorbent for enhanced removal of Cr(VI) in aqueous solutions by adsorption combined with reduction, Chemical Engineering Journal. 408 (2021) 127281. doi:10.1016/j.cej.2020.127281.

[14] J. Sun, Y. Hou, Z. Yu, L. Tu, Y. Yan, S. Qin, S. Chen, D. Lan, H. Zhu, S. Wang, Visible-light-driven Z-scheme Zn3In2S6/AgBr photocatalyst for boosting simultaneous Cr (VI) reduction and metronidazole oxidation: Kinetics, degradation pathways and mechanism, Journal of Hazardous Materials. (2021) 126543. doi:10.1016/j.jhazmat.2021.126543.

[15] Y. Liu, D. Yang, T. Xu, Y. Shi, L. Song, Z.Z. Yu, Continuous photocatalytic removal of chromium (VI) with structurally stable and porous Ag/Ag3PO4/reduced graphene oxide microspheres, Chemical Engineering Journal. 379 (2020) 122200. doi:10.1016/j.cej.2019.122200.

[16] D. Lu, P. Fang, W. Wu, J. Ding, L. Jiang, X. Zhao, C. Li, M. Yang, Y. Li, D. Wang, Solvothermal-assisted synthesis of self-assembling TiO2 nanorods on large graphitic carbon nitride sheets with their anti-recombination in the photocatalytic removal of Cr(VI) and rhodamine B under VIsible light irradiation, Nanoscale. 9 (2017) 3231–3245. doi:10.1039/c6nr09137g.

[17] L.W. Duresa, D.H. Kuo, K.E. Ahmed, M.A. Zeleke, H. Abdullah, Highly enhanced photocatalytic Cr(vi) reduction using In-doped Zn(O,S) nanoparticles, New Journal of Chemistry. 43 (2019) 8746–8754. doi:10.1039/c9nj01511f.

[18] Y. Yang, L. Yan, J. Li, J. Li, T. Yan, M. Sun, Z. Pei, Synergistic adsorption and photocatalytic reduction of Cr(VI) using Zn-Al-layered double hydroxide and TiO2 composites, Applied Surface Science. 492 (2019) 487–496. doi:10.1016/j.apsusc.2019.06.229.

[19] Q. Xia, B. Huang, X. Yuan, H. Wang, Z. Wu, L. Jiang, T. Xiong, J. Zhang, G. Zeng,

H. Wang, Modified stannous sulfide nanoparticles with metal-organic framework: Toward efficient and enhanced photocatalytic reduction of chromium (VI) under visible light, Journal of Colloid and Interface Science. 530 (2018) 481–492. doi:10.1016/j.jcis.2018.05.015.

[20] C.R. Chen, H.Y. Zeng, S. Xu, J.C. Shen, G. Hu, R.L. Zhu, J.Z. Du, Y.X. Sun, Facile fabrication of CdS/ZnAlO heterojunction with enhanced photocatalytic activity for Cr(VI) reduction under visible light, Applied Clay Science. 165 (2018) 197–204. doi:10.1016/j.clay.2018.08.019.

[21] Z. Chen, Y. Luo, C. Huang, X. Shen, In situ assembly of ZnO/graphene oxide on synthetic molecular receptors: Towards selective photoreduction of Cr(VI) via interfacial synergistic catalysis, Chemical Engineering Journal. 414 (2021) 128914. doi:10.1016/j.cej.2021.128914.

[22] Y. Sun, L. Xu, P. Jin, X. Bai, X. Jin, X. Shi, Simultaneous removal of colorless micropollutants and hexavalent chromium by pristine TiO2 under visible light: An electron transfer mechanism, Chemical Engineering Journal. 405 (2021) 126968. doi:10.1016/j.cej.2020.126968.

[23] L. Hou, Y. Zhang, Y. Ma, Y. Wang, Z. Hu, Y. Gao, Z. Han, Reduced Phosphomolybdate Hybrids as Efficient Visible-Light Photocatalysts for Cr(VI) Reduction, Inorganic Chemistry. 58 (2019) 16667–16675. doi:10.1021/acs.inorgchem.9b02777.

[24] M. Naguib, M. Kurtoglu, V. Presser, J. Lu, J. Niu, M. Heon, L. Hultman, Y. Gogotsi, M.W. Barsoum, Two-Dimensional Nanocrystals Produced by Exfoliation of Ti3AlC2, Advanced Materials. 23 (2011) 4248–4253. doi:10.1002/adma.201102306.

[25] M. Alhabeb, K. Maleski, B. Anasori, P. Lelyukh, L. Clark, S. Sin, Y. Gogotsi, Guidelines for Synthesis and Processing of Two-Dimensional Titanium Carbide (Ti3C2Tx MXene), Chemistry of Materials. 29 (2017) 7633–7644. doi:10.1021/acs.chemmater.7b02847.

[26] J. Lao, R. Lv, J. Gao, A. Wang, J. Wu, J. Luo, Aqueous Stable Ti 3 C 2 MXene Membrane with Fast and Photoswitchable Nanofluidic Transport, ACS Nano. 12 (2018) 12464–12471. doi:10.1021/acsnano.8b06708.

[27] S. Kim, M. Yu, Y. Yoon, Fouling and Retention Mechanisms of Selected Cationic and Anionic Dyes in a Ti3C2Tx MXene-Ultrafiltration Hybrid System, ACS Applied Materials and Interfaces. 12 (2020) 16557–16565.

doi:10.1021/acsami.0c02454.

[28] B. Zielińska, A. Wróblewska, K. Maślana, P. Miądlicki, K. Kiełbasa, A. Rozmysłowska-Wojciechowska, M. Petrus, J. Woźniak, A.M. Jastrzębska, B. Michalkiewicz, E. Mijowska, High catalytic performance of 2D Ti3C2Tx MXene in α-pinene isomerization to camphene, Applied Catalysis A: General. 604 (2020) 117765. doi:10.1016/j.apcata.2020.117765.

[29] V. Sharma, A. Kumar, A. Kumar, V. Krishnan, Enhanced photocatalytic activity of two dimensional ternary nanocomposites of ZnO–Bi2WO6–Ti3C2 MXene under natural sunlight irradiation, Chemosphere. 287 (2022). doi:10.1016/J.CHEMOSPHERE.2021.132119.

[30] X. Feng, Z. Yu, Y. Sun, R. Long, M. Shan, X. Li, Y. Liu, J. Liu, Review MXenes as a new type of nanomaterial for environmental applications in the photocatalytic degradation of water pollutants, Ceramics International. (2020). doi:10.1016/j.ceramint.2020.11.151.

[31] C. Prasad, X. Yang, Q. Liu, H. Tang, A. Rammohan, S. Zulfiqar, G. V. Zyryanov, S. Shah, Recent advances in MXenes supported semiconductors based photocatalysts: Properties, synthesis and photocatalytic applications, Journal of Industrial and Engineering Chemistry. 85 (2020) 1–33. doi:10.1016/j.jiec.2019.12.003.

[32] B. Sun, P. Qiu, Z. Liang, Y. Xue, X. Zhang, L. Yang, H. Cui, J. Tian, The fabrication of 1D/2D CdS nanorod@Ti3C2 MXene composites for good photocatalytic activity of hydrogen generation and ammonia synthesis, Chemical Engineering Journal. 406 (2021) 127177. doi:10.1016/j.cej.2020.127177.

[33] Y. Ying, Y. Liu, X. Wang, Y. Mao, W. Cao, P. Hu, X. Peng, Two-dimensional titanium carbide for efficiently reductive removal of highly toxic chromium(VI) from water, ACS Applied Materials and Interfaces. 7 (2015) 1795–1803. doi:10.1021/am5074722.

[34] Z. Li, Y. Wu, 2D Early Transition Metal Carbides (MXenes) for Catalysis, Small. 15 (2019) 1804736. doi:10.1002/SMLL.201804736.

[35] H. Wang, Y. Sun, Y. Wu, W. Tu, S. Wu, X. Yuan, G. Zeng, Z.J. Xu, S. Li, J.W. Chew, Electrical promotion of spatially photoinduced charge separation via interfacial-built-in quasi-alloying effect in hierarchical Zn2In2S5/Ti3C2(O, OH)x hybrids toward efficient photocatalytic hydrogen evolution and environmental remediation, Applied Catalysis B: Environmental. 245 (2019) 290–301.

doi:10.1016/j.apcatb.2018.12.051.

[36] A. Shahzad, K. Rasool, W. Miran, M. Nawaz, J. Jang, K.A. Mahmoud, D.S. Lee, Two-Dimensional Ti3C2Tx MXene Nanosheets for Efficient Copper Removal from Water, ACS Sustainable Chemistry and Engineering. 5 (2017) 11481–11488. doi:10.1021/acssuschemeng.7b02695.

[37] Q. Peng, J. Guo, Q. Zhang, J. Xiang, B. Liu, A. Zhou, R. Liu, Y. Tian, Unique lead adsorption behavior of activated hydroxyl group in two-dimensional titanium carbide, Journal of the American Chemical Society. 136 (2014) 4113–4116. doi:10.1021/ja500506k.

[38] A. Shahzad, K. Rasool, W. Miran, M. Nawaz, J. Jang, K.A. Mahmoud, D.S. Lee, Mercuric ion capturing by recoverable titanium carbide magnetic nanocomposite, Journal of Hazardous Materials. 344 (2018) 811–818. doi:10.1016/j.jhazmat.2017.11.026.

[39] K. Fu, X. Liu, D. Yu, J. Luo, Z. Wang, J.C. Crittenden, Highly Efficient and Selective Hg(II) Removal from Water Using Multilayered Ti3C2O xMXene via Adsorption Coupled with Catalytic Reduction Mechanism, Environmental Science and Technology. 54 (2020) 16212–16220. doi:10.1021/acs.est.0c05532.

[40] P. Karthikeyan, K. Ramkumar, K. Pandi, A. Fayyaz, S. Meenakshi, C.M. Park, Effective removal of Cr(VI) and methyl orange from the aqueous environment using two-dimensional (2D) Ti3C2Tx MXene nanosheets, Ceramics International. 47 (2021) 3692–3698. doi:10.1016/J.CERAMINT.2020.09.221.

[41] Y. Tang, C. Yang, W. Que, A novel two-dimensional accordion-like titanium carbide (MXene) for adsorption of Cr(VI) from aqueous solution, Journal of Advanced Dielectrics. 8 (2018) 1850035. doi:10.1142/S2010135X18500352.

[42] A. Kong, Y. Sun, M. Peng, H. Gu, Y. Fu, J. Zhang, W. Li, Amino-functionalized MXenes for efficient removal of Cr(VI), Colloids and Surfaces A: Physicochemical and Engineering Aspects. 617 (2021) 126388. doi:10.1016/j.colsurfa.2021.126388.

[43] O. Mashtalir, K.M. Cook, V.N. Mochalin, M. Crowe, M.W. Barsoum, Y. Gogotsi, Dye adsorption and decomposition on two-dimensional titanium carbide in aqueous media, Journal of Materials Chemistry A. 2 (2014) 14334–14338. doi:10.1039/C4TA02638A.

[44] M. Rosales, A. Garcia, V.M. Fuenzalida, R. Espinoza-González, G. Song, B. Wang, J. Yu, F. Gracia, A. Rosenkranz, Unprecedented arsenic photo-oxidation behavior of few- and multi-layer Ti3C2Tx nano-sheets, Applied Materials Today. 20 (2020)

100769. doi:10.1016/j.apmt.2020.100769.

[45] D. Zhao, C. Cai, Preparation of Bi2MoO6/Ti3C2MXene heterojunction photocatalysts for fast tetracycline degradation and Cr(vi) reduction, Inorganic Chemistry Frontiers. 7 (2020) 2799–2808. doi:10.1039/d0qi00540a.

[46] N.H. Alias, J. Jaafar, S. Samitsu, N. Yusof, M.H.D. Othman, M.A. Rahman, A.F. Ismail, F. Aziz, W.N.W. Salleh, N.H. Othman, Photocatalytic degradation of oilfield produced water using graphitic carbon nitride embedded in electrospun polyacrylonitrile nanofibers, Chemosphere. 204 (2018) 79–86. doi:10.1016/j.chemosphere.2018.04.033.

[47] A. Lace, D. Ryan, M. Bowkett, J. Cleary, Chromium Monitoring in Water by Colorimetry Using Optimised 1,5-Diphenylcarbazide Method, International Journal of Environmental Research and Public Health. 16 (2019). doi:10.3390/IJERPH16101803.

[48] C. Peng, P. Wei, X. Chen, Y. Zhang, F. Zhu, Y. Cao, H. Wang, H. Yu, F. Peng, A hydrothermal etching route to synthesis of 2D MXene (Ti3C2, Nb2C): Enhanced exfoliation and improved adsorption performance, Ceramics International. 44 (2018) 18886–18893. doi:10.1016/j.ceramint.2018.07.124.

[49] G.P. Lim, C.F. Soon, M. Morsin, M.K. Ahmad, N. Nayan, K.S. Tee, Synthesis, characterization and antifungal property of Ti3C2Tx MXene nanosheets, Ceramics International. 46 (2020) 20306–20312. doi:10.1016/j.ceramint.2020.05.118.

[50] W. Feng, H. Luo, Y. Wang, S. Zeng, L. Deng, X. Zhou, H. Zhang, S. Peng, Ti3C2 MXene: A promising microwave absorbing material, RSC Advances. 8 (2018) 2398–2403. doi:10.1039/c7ra12616f.

[51] X. Gao, Z.K. Li, J. Xue, Y. Qian, L.Z. Zhang, J. Caro, H. Wang, Titanium carbide Ti3C2Tx (MXene) enhanced PAN nanofiber membrane for air purification, Journal of Membrane Science. 586 (2019) 162–169. doi:10.1016/j.memsci.2019.05.058.

[52] J. Chen, X. Yuan, F. Lyu, Q. Zhong, H. Hu, Q. Pan, Q. Zhang, Integrating MXene nanosheets with cobalt-tipped carbon nanotubes for an efficient oxygen reduction reaction, Journal of Materials Chemistry A. 7 (2019) 1281–1286. doi:10.1039/c8ta10574j.

[53] J. Zhu, Y. Tang, C. Yang, F. Wang, M. Cao, Composites of TiO 2 Nanoparticles Deposited on Ti 3 C 2 MXene Nanosheets with Enhanced Electrochemical Performance , Journal of The Electrochemical Society. 163 (2016) A785–A791. doi:10.1149/2.0981605jes.

[54] L. Wang, B. Shi, Hydroxide conduction enhancement of chitosan membranes by functionalized MXene, Materials. 11 (2018). doi:10.3390/ma11112335.

[55] S. Alekseev, D. Korytko, M. Iazykov, S. Khainakov, V. Lysenko, Electrochemical Synthesis of Carbon Fluorooxide Nanoparticles from 3C-SiC Substrates, Journal of Physical Chemistry C. 119 (2015) 20503–20514. doi:10.1021/acs.jpcc.5b06524.

[56] U. Khalil, M.B. Shakoor, S. Ali, S.R. Ahmad, M. Rizwan, A.A. Alsahli, M.N. Alyemeni, Selective removal of hexavalent chromium from wastewater by rice husk: Kinetic, isotherm and spectroscopic investigation, Water (Switzerland). 13 (2021) 263. doi:10.3390/w13030263.

[57] T.D. Ntuli, T.H. Mongwe, L.L. Sikeyi, O. Mkhari, N.J. Coville, E.N. Nxumalo, M.S. Maubane-Nkadimeng, Removal of hexavalent chromium via an adsorption coupled reduction mechanism using olive oil derived carbon nano-onions, Environmental Nanotechnology, Monitoring and Management. 16 (2021) 100477. doi:10.1016/j.enmm.2021.100477.

[58] M. Shirzad-Siboni, M. Farrokhi, R. Darvishi Cheshmeh Soltani, A. Khataee, S. Tajassosi, Photocatalytic reduction of hexavalent chromium over ZnO nanorods immobilized on kaolin, Industrial and Engineering Chemistry Research. 53 (2014) 1079–1087. doi:10.1021/ie4032583.

[59] D. Jiang, Y. Yang, C. Huang, M. Huang, J. Chen, T. Rao, X. Ran, Removal of the heavy metal ion nickel (II) via an adsorption method using flower globular magnesium hydroxide, Journal of Hazardous Materials. 373 (2019) 131–140. doi:10.1016/j.jhazmat.2019.01.096.

[60] N.H. Mthombeni, S. Mbakop, S.C. Ray, T. Leswifi, A. Ochieng, M.S. Onyango, Highly efficient removal of chromium (VI) through adsorption and reduction: A column dynamic study using magnetized natural zeolite-polypyrrole composite, Journal of Environmental Chemical Engineering. 6 (2018) 4008–4017. doi:10.1016/j.jece.2018.05.038.

[61] A.L. Popovic, J.D. Rusmirovic, Z. Velickovic, T. Kovacevic, A. Jovanovic, I. Cvijetic, A.D. Marinkovic, Kinetics and column adsorption study of diclofenac and heavy-metal ions removal by amino-functionalized lignin microspheres, Journal of Industrial and Engineering Chemistry. 93 (2021) 302–314. doi:10.1016/j.jiec.2020.10.006.

[62] Q.H. Li, M. Dong, R. Li, Y.Q. Cui, G.X. Xie, X.X. Wang, Y.Z. Long, Enhancement of Cr(VI) removal efficiency via adsorption/photocatalysis synergy using

electrospun chitosan/g-C3N4/TiO2 nanofibers, Carbohydrate Polymers. 253 (2021) 117200. doi:10.1016/j.carbpol.2020.117200.

[63] P.C. Okafor, C.O. Obadimu, Solar Photocatalytic Degradation of Phenol Using Cocos Nucifera (Coconut) Shells as Adsorbent, (2015). doi:10.15640/jcb.v3n1a3.

[64] N.K. Mondal, S. Chakraborty, Adsorption of Cr(VI) from aqueous solution on graphene oxide (GO) prepared from graphite: equilibrium, kinetic and thermodynamic studies, Applied Water Science. 10 (2020). doi:10.1007/S13201-020-1142-2.

[65] J. Bu, W. Li, N. Niu, N. Guo, H. Zhou, C. Chen, A. Ding, Adsorption of Cr(VI) from wastewater by iron-modified coconut shell biochar, E3S Web of Conferences. 248 (2021). doi:10.1051/E3SCONF/202124801059.

[66] S. Singh, A.G. Anil, S. Khasnabis, V. Kumar, B. Nath, V. Adiga, T.S.S. Kumar Naik, S. Subramanian, V. Kumar, J. Singh, P.C. Ramamurthy, Sustainable removal of Cr(VI) using graphene oxide-zinc oxide nanohybrid: Adsorption kinetics, isotherms and thermodynamics, Environmental Research. 203 (2022) 111891. doi:10.1016/J.ENVRES.2021.111891.

[67] M. Malakootian, F. Mansuri, Hexavalent chromium removal by titanium dioxide photocatalytic reduction and the effect of phenol and humic acid on its removal efficiency, International Journal of Environmental Health Engineering. 4 (2015) 19. doi:10.4103/2277-9183.157720.

[68] S. Mor, K. Ravindra, N.R. Bishnoi, Adsorption of chromium from aqueous solution by activated alumina and activated charcoal, Bioresource Technology. 98 (2007) 954–957. doi:10.1016/J.BIORTECH.2006.03.018.

[69] I.-I.N. Etim, P.C. Okafor, R.A. Etiuma, C.O. Obadimu, Solar Photocatalytic Degradation of Phenol Using Cocos Nucifera (Coconut) Shells as Adsorbent, Journal of Chemistry and Biochemistry. 3 (2015). doi:10.15640/jcb.v3n1a3.

[70] X. Wang, Y. Liang, W. An, J. Hu, Y. Zhu, W. Cui, Removal of chromium (VI) by a self-regenerating and metal free g-C3N4/graphene hydrogel system via the synergy of adsorption and photo-catalysis under visible light, Applied Catalysis B: Environmental. 219 (2017) 53–62. doi:10.1016/j.apcatb.2017.07.008.

[71] A. Jain, A. Kumar, H. Kaur, V. Krishnan, Strategic combination of ultra violet-visible-near infrared light active materials towards maximum utilization of full solar spectrum for photocatalytic chromium reduction, Chemosphere. 267 (2021) 128884. doi:10.1016/J.CHEMOSPHERE.2020.128884.